Biofuel Research Journal 26 (2020) 1159-1169

BRTeam BIOFUEL RESEARCH TEAM

Biofuel Research Journal

Journal homepage: www.biofueljournal.com



Original Research Paper

Qualitative role of heterogeneous catalysts in biodiesel production from *Jatropha curcas* oil

Fatai Alade Aderibigbe [1,*], Sherif Ishola Mustapha [1,2], Tunmise Latifat Adewoye [1], Ishaq Alhassan Mohammed [1], Adebola Bukola Gbadegesin [1], Faith Emmanuel Niyi [1], Opeyemi Idowu Olowu [1], Akinpelumi Gabriel Soretire [1], Harvis Bamidele Saka [1]

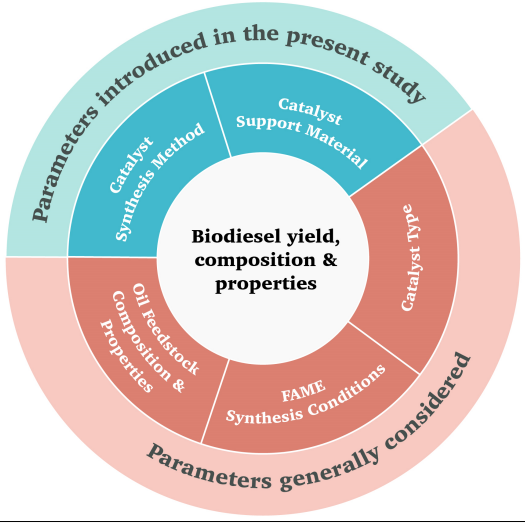
[1]*Department of Chemical Engineering, Faculty of Engineering and Technology, University of Ilorin, Ilorin, Nigeria.*

[2]*Department of Chemical Engineering, Durban University of Technology, South Africa*.

HIGHLIGHTS

- Tri-metallic (Fe-Co-Ni) catalyst was synthesized through two different techniques; green synthesis and wet impregnation.
- Impacts of synthsis method and support material on final bioduesel product was scrutinized.
- Catalyst support material/synthesis method influenced the yield of the produced biodiesel.
- Catalyst support/synthesis method influenced the composition and propeties of the resultant biodiesel.
- Green-synthesized Fe-Co-Ni-MgO catalyst led to highest biodiesel yield of 97.9%

GRAPHICAL ABSTRACT



ARTICLE INFO

Article history:
Received 19 December 2019
Received in revised form 26 March 2020
Accepted 27 March 2020
Available online 1 June 2020

Keywords:
Green synthesis
Wet impregnation
Jatropha curcas oil
Biodiesel
Unsaturation
FAME profile

ABSTRACT

Biodiesel properties are in general attributed to the composition and properties of the oil feedstock used, overlooking the possible impacts of the catalyst preparation details. In light of that, the impacts of different catalyst preparation techniques alongside those of different support materials on the yield, composition, and fuel properties of biodiesels produced from the same oil feedstock were investigated. More specifically, tri-metallic (Fe-Co-Ni) catalyst was synthesized through two different techniques (green synthesis and wet impregnation) using MgO or ZnO as support material. The generated catalyst pairs, i.e., *Fe-Co-Ni/MgO* and *Fe-Co-Ni/ZnO* prepared by wet impregnation and *Fe-Co-Ni-MgO* and *Fe-Co-Ni-ZnO* prepared by green synthesis (using leaf extracts) were used in the transesterification process of *Jatropha curcas* oil. Detailed morphological properties, composition, thermal stability, crystalline nature, and functional groups characterization of the catalysts were also carried out. Using Box-Behnken Design response surface methodology, it was found that the green-synthesized *Fe-Co-Ni-MgO* catalyst resulted in the highest biodiesel yield of 97.9%. More importantly, the fatty acid methyl ester (FAME) profiles of the biodiesels produced using the four catalysts as well as their respective fuel properties were different in spite of using the same oil feedstock.

© 2020 BRTeam. All rights reserved.

* Corresponding authors at: Tel.: +234 8033822123
E-mail address: aderibigbe.fa@unilorin.edu.ng

Please cite this article as: Aderibigbe F.A., Mustapha S.I., Adewoye T.L., Mohammed I.A., Gbadegesin A.B., Niyi F.E., Olowu O.I., Soretire A.G., Saka H.B. Qualitative role of heterogeneous catalysts in biodiesel production from *Jatropha curcas* oil. Biofuel Research Journal 26 (2020) 1159-1169. DOI: 10.18331/BRJ2020.7.2.4

1. Introduction

There have been several literature reports on the influences that biodiesel chemical structure such as its degree of unsaturation could have on engine performance, combustion, and emissions characteristics (Lapuerta et al., 2009; Benjumea et al., 2010; Sokoto et al., 2011; Altun, 2014; Yang et al., 2016; Hellier et al., 2017; Folayan et al., 2019). For instance, the work of Benjumea et al. (2010) has shown that a higher degree of unsaturation of biodiesel fuels causes a more retarded start of combustion, while Gopinath et al. (2010) showed that biodiesels having more unsaturated fatty acids emit more oxides of nitrogen and exhibit lower thermal efficiency compared to biodiesels having more saturated acids.

Overall, biodiesel properties depend on the properties of the various individual fatty esters constituting the fuel which are in turn determined by the structural features of their fatty acid and alcohol moieties (Refaat, 2009). Exactly for this reason, factors such as molecular structure and composition of the oil feedstocks and alcohols are principally considered to optimize the performance of the final biodiesel fuel (Refaat, 2009). Extensive studies on various oils have considered the use of different catalysts to obtain biodiesels of specific fatty acid methyl ester (FAME) profiles and qualities (Omotoso et al., 2011; Sharmila et al., 2016; Gupta and Agarwal, 2016; Cruz-Ortiz and Ríos-González, 2017). Commonly, these studies conclude that the oils used are responsible for the chemical structures and properties of the produced biodiesel. However, there seem to be some ambiguities as the possible involvement of catalyst type and synthesis route in determining FAME profiles is not generally monitored nor reported on in these studies. Consequently, from most of the previous investigations, it is difficult to infer the exact role of catalysts and their selectivity towards the formation of particular methyl ester molecules.

It should also be noted that the quantitative role of catalysts (i.e., impact on yield) has been the focus of many past studies and been properly addressed (Kaisan et al., 2016; Sharma et al., 2018). While the qualitative impacts of catalysts in influencing the type of methyl esters (saturated/unsaturated) were largely ignored possibly due to the fact that oil feedstock and its fatty acid profile is regarded as the most important parameter.

Currently, the state-of-art in rational design of catalysts involves the development of predictive models using different computational methods and their validation with experiments (synthesis, characterization, and performance tests). Machine learning algorithms are particularly useful as they can find complex correlations from large data sets. Catalysts exhibit complex structure–property–activity relationship, thus an efficient means of discovering improved catalysts is with the rational design of catalysts since physical insights are combined with data to construct predictive models, which lead to design principles for identifying promising candidate catalysts. Systematic experiments are then performed for validating the activity of a predicted catalyst, providing further physical insights while assisting with refining the predictive models and design principles (Tsai, 2017). Existing computational heterogeneous catalysis tools include predictive modeling, density functional theory (DFT), scaling correlations (adsorption scaling relations and transition state energies), micro-kinetic modeling, and volcano relations (descriptor-based models). A good review of the general optimization framework for rational design of catalysts can be found in Wang and Hu (2016) and Tsai (2017).

Yet, the future of heterogeneous catalysis is faced with our limited understanding of catalysts' behavior under dynamic reaction conditions (Kalz et al., 2017). The structure of catalysts is very dynamic and in-depth studies of catalysts and catalytic reactors under such transient conditions have only started recently. For instance, the generation of corresponding pool of candidate structures is already a daunting task for steady-state operation and will not become easier for dynamic operation (Kalz et al., 2017). Kalz et al. (2017) suggests an intensive exchange between the fields of 1) operando spectroscopy including time-resolved methods, 2) theory with predictive quality, 3) kinetic modelling, 4) design of catalysts by appropriate preparation concepts, and 5) novel/modular reactor designs, to address the challenges faced.

In biodiesel production, heterogeneous catalysts are preferred because they are more economical given their easy separation from the reaction mixture and reusability (Al-Muhtaseb et al., 2018). Moreover, biodiesel production can be eco-friendlier and more economic if such catalysts are utilized (Al-Muhtaseb et al., 2018).

Bimetallic heterogeneous catalysts have been well studied for a wide range of applications in energy production and environmental remediation due to their tunable properties which are governed by compositions of the metallic systems, preparation method, and morphostructure (De et al., 2016). Such bimetallic catalysts as Ca/Fe (Kwong and Yung, 2015), Au-Ag (Banerjee et al., 2014), Ni-W supported on Al-MCM-41 (Yang et al., 2019), W-Zr/CaO (Nasar and Taufiq-Yap, 2017), Mo–Mn, Mo–Zn, and Mo–Sn supported on γ-Al_2O_3-MgO (Farooq et al., 2016) have been studied and were found efficient for the production of biodiesel. Nevertheless, trimetallic catalysts have been reported to offer superior catalytic properties compared to the mono- and bimetallic types (Yin et al., 2017). For instance, the superior catalytic performance of Fe-Co-Ni catalyst over Fe-Co, Fe-Ni, Co-Ni or their monometallic forms was experimentally shown by Abdulkareem et al. (2017). Recently, ternary and quaternary metal complexes such as Cu/Ni/Ca/Al_2O_3 and Cu/Zn/Ca/Al_2O_3 were shown to be capable of producing methyl esters with high yield and quality (Kamal, 2018).

Our lack of sufficient understanding in this emerging field necessitates further studies to obtain more in-depth insights. Therefore, trimetallic transition metal catalysts, delineated across support materials, were prepared by wet impregnation and green synthesis methods and were used to produce biodiesel from physic nut (*Jatropha curcas*) oil. More specifically, the impacts of different catalysts on the degree of unsaturation and FAME profiles of biodiesels produced from an identical oil feedstock were investigated. The findings could pave the way for more rational design of heterogeneous catalysts using any of the several available optimization frameworks to obtain catalysts with features of interest.

2. Materials and Methods

2.1. Materials

Analytical grade chemicals (Sigma-Aldrich) were used in this study. The *J. curcas* oil used was obtained from the University of Ilorin *J. curcas* plantation. Other materials used are *Amaranthus spinopus* leaves, *Citrus aurantifolia* leaves, phenolphthalein (indicator), distilled water, de-ionized water and paper foil.

2.2. Methodology

2.2.1. Determination of acid value and free fatty acid of Jatropha Curcas oil

To determine the acid value, 25 mL of ethanol was added to diethyl ether (25 mL) and the mixture was then mixed with 0.1M NaOH. A few drops of phenolphthalein solution serving as the indicator was also added. About 10 g of *J. curcas* oil was dissolved in the mixture followed by titration against 0.1M NaOH until a pink color was obtained. The acid values and the percentage of free fatty acid (FFA%) were measured according to standard methods (Gardy et al., 2010), using **Equations 1** and **2**:

$$Acid\ value\ \left(\frac{mgKOH}{g}\right) = \frac{(V_{bs}-V_b)\times C\times 56.11}{W} \quad \text{(Eq. 1)}$$

$$Free\ fatty\ acid\ (\%) = \frac{(V_{bs}-V_b)\times C\times 28.246}{W} \quad \text{(Eq. 2)}$$

where V_{bs} is the consumed volume of titrate for biodiesel sample (mL); V_b denotes the consumed volume of titrate for the blank (mL); C stands for the exact concentration of standardized alcoholic potassium hydroxide solution (mole/L), and W is the mass of biodiesel sample used (g).

2.2.2. Preparation of catalysts

Tri-metallic catalyst of iron, cobalt, and nickel supported on magnesium oxide was prepared by the wet impregnation technique (*Fe-Co-Ni/MgO*) and a green synthesis route using a plant extract (*Fe-Co-Ni-MgO*). Moreover, tri-metallic catalyst of iron, cobalt, and nickel supported on zinc oxide was prepared by the wet impregnation technique (*Fe-Co-Ni/ZnO*) and the green synthesis route (*Fe-Co-Ni-ZnO*).

Please cite this article as: Aderibigbe F.A., Mustapha S.I., Adewoye T.L., Mohammed I.A., Gbadegesin A.B., Niyi F.E., Olowu O.I., Soretire A.G., Saka H.B. Qualitative role of heterogeneous catalysts in biodiesel production from *Jatropha curcas* oil. Biofuel Research Journal 26 (2020) 1159-1169. DOI: 10.18331/BRJ2020.7.2.4

(a) Wet impregnation synthesis of Fe-Co-Ni/MgO and Fe-Co-Ni/ZnO catalysts

The *Fe-Co-Ni/MgO* or *Fe-Co-Ni/ZnO* catalyst was prepared by dissolving equimolar quantities of the nitrate salts of Fe, Co, and Ni (1:1:1) in deionized water followed by mixing with 16 g of MgO or ZnO. The mixture was allowed to stand for 60 min, and followed by drying at 120°C for 8 h. It was subsequently screened with a 150 µm sieve, and was calcined at 500°C for 3 h.

(b) Green synthesis of Fe-Co-Ni-MgO catalyst

First, unripe leaves of *A. spinosus* were collected and washed thoroughly with distilled water. The fresh leaves were chopped into small pieces and were subsequently reduced to a paste using a mortar and pestle. The fine paste was used in the preparation of the leaf extract. Distilled water (100 mL) was added to 20 g of the paste which was transferred carefully into a 250 mL Erlenmeyer flask and was magnetically stirred at 100°C for 30 min. The extract obtained was filtered and the clear extract was stored for use in the synthesis of colloidal MgO particles. The extract was characterized using Fourier-transform infrared spectroscopy (FTIR) spectroscopy to check for the various functional groups present.

An equimolar solution of iron, cobalt, and nickel nitrates (1:1:1) was prepared, stirred at 50°C for 30 min using a magnetic stirrer, dried at 120°C for about 2 h, and was finally calcined at 500°C for 3 h. The sample was stored for future use to provide the Fe, Co, and Ni active metals of the catalyst.

A 1 M solution of $Mg(NO_3)_2{\cdot}6H_2O$ was prepared as the source for magnesium oxide nanoparticles, stirred at 50°C for about 10 min using a magnetic stirrer to allow for the proper mixing of the solution. Then, 50 mL of the prepared leaf extract solution was added to the solution while continuously stirred magnetically. The color of the mixture was found to be greenish at first but after being stirred continuously for about 20 min, a marked reduction in the intensity of the color was noticed. The UV-Vis spectrum of the mixture was then recorded to confirm the formation of the MgO nanoparticles (**Fig. S1**).

Finally, the *Fe-Ni-Co-MgO* catalyst was prepared by adding 3 g of the calcined sample to the mixture containing the MgO nanoparticles and stirred magnetically at 50°C for about 20 min to increase the homogeneity of the sample. This mixture was then dried at 120°C for 2 h and was subsequently calcined at 500°C for 3 h. The calcined material was recovered and stored for use in the biodiesel production process.

(c) Green synthesis of Fe-Co-Ni-ZnO catalyst

The *Fe-Co-Ni-ZnO* catalyst was prepared by hybridization in which the Fe, Ni, and Co were obtained by direct dissolution and mixing of their nitrate salts in deionized water, while ZnO was derived from the reduction of its nitrate salt by the whole extract of *C. aurantifolia* leaves. The unripe leaves of *C. aurantifolia* were collected, washed thoroughly with distilled water, and reduced in size using a mortar and pestle. Then, 20 g of the mashed *C. aurantifolia* leaves was added to 100 mL of distilled water in a 250 mL Erlenmeyer flask and stirred at 100°C for 30 min using a magnetic stirrer. The obtained extract was mixed and filtered. The filtrate was kept in the refrigerator until use. The leaf extract was characterized by the FTIR spectroscopy to identify the functional groups present in the sample.

Zinc nitrate hexahydrate, $Zn(NO_3)_2{\cdot}6H_2O$, served as the precursor for synthesis of ZnO nanoparticles. The precursor solution was prepared by dissolving 20 g of Zn $(NO_3)_2.6H_2O$ in 50 mL of distilled water. This solution was then stirred at 50ºC for 30 min using a magnetic stirrer. Thereafter, about 50 mL of leaf extract was added to the solution and this mixture was boiled until it was reduced to a deep yellow colored paste.

The sources of iron, cobalt, and nickel metals in the catalyst were their corresponding nitrate salts, i.e., $Fe(NO_3)_3{\cdot}9H_2O$, $Co(NO_3)_2{\cdot}6H_2O$, and Ni $(NO_3)_2{\cdot}6H_2O$). A 0.01 M precursor solution containing Fe, Co, and Ni (1:1:1) was prepared, and stirred at 50°C for 30 min using a magnetic stirrer. The mixture was dried for 3 h and calcined at 400ºC for 3 h resulting in a fine black powder.

The *Fe-Ni-Co-ZnO* catalyst was finally prepared by mixing the calcined material (fine black powder) with the deep yellow colored paste obtained from zinc nitrate, and was stirred at 50ºC for 30 min. The mixture was then calcined at 500ºC for 2 h.

2.2.3. Characterization of catalysts

The four synthesized catalysts: (a) *Fe-Co-Ni/MgO*, (b) *Fe-Co-Ni-MgO*, (c) *Fe-Co-Ni/ZnO*, and (d) *Fe-Co-Ni-ZnO* were characterized for their crystalline nature, morphological properties, elemental compositions, functional groups, and thermal stability using X-ray powder diffraction (XRD), scanning electron microscope with an energy dispersive X-ray spectrometer (SEM-EDS), FTIR, and thermal gravimetric analysis (TGA), respectively. The XRD analysis was performed on a Bruker AXS D8 Advance (USA) with Cu-Kα radiation. A portion of the crystals were sprinkled on a de-greased glass slide, and diffractograms were recorded between diffraction angles of 15º and 80º. The SEM morphology results of the synthesized catalysts were acquired using a high-resolution Zeiss Auriga (USA). A crystal sample (1 mg) was sprinkled onto a carbon adhesive tape and sputter coated with Au-Pd using a Quorum T15OT for 5 min prior to the analysis. The microscope was operated with an electron high tension at 5 kV for imaging. In the FTIR analysis, infrared light in the range 500–4000 cm^{-1} was used to scan the sample. The sample was prepared using a standard potassium bromide (KBr) and was then placed on a crystal in the Nicholet iS5 spectrometer. In the TGA procedure, small quantity of the sample was placed on the sample pan and the TGA-DSC analysis was performed using a TGA SDT Q600 instrument (TA Instruments). The programmed heating range was from room temperature (30ºC) to 800ºC at the rate of 10 $ºC.min^{-1}$ under nitrogen atmosphere.

2.2.4. Optimization of biodiesel production

The catalysts (*Fe-Co-Ni/MgO*, *Fe-Co-Ni/ZnO*, *Fe-Co-Ni-MgO*, and *Fe-Co-Ni-ZnO*) as prepared were employed in producing biodiesel using *J. curcas* oil and methanol. From several experimental runs conducted (**Table 1**), optimal conditions for biodiesel yield were identified for each of the catalysts used. Optimization of biodiesel production was performed using Box-Behnken Design (BBD), a response surface methodology by varying the reaction temperature, reaction time, methanol to oil molar ratio, and catalyst concentration.

Table 1.
Design of experiment for biodiesel production.

Factors	Temperature (°C)	MeOH:Oil molar ratio (w/w)	Catalyst concentration (% w/w of oil)	Reaction time (h)
Level 1	50	10: 1	5	1
Level 2	55	15: 1	10	2
Level 3	60	20: 1	15	3

Experiments were carried out in 20 mL test tubes placed in a water bath shaker with a constant temperature. In a typical run, 1 g of *J. curcas* oil was measured into the test tube. Then, 2 mL of hexane was added to the oil to serve as a co-solvent and enhance the miscibility of oil with methanol and to speed up the rate of transesterification. Known amounts of catalyst (5%, 10%, or 15% w/w of oil) and methanol (methanol to oil ratio; 10:1, 15:1, or 20:1) were added to the mixture and stirred vigorously using a constant agitation speed, while maintained at a certain temperature (50, 55, or 60ºC) and for a certain reaction duration (1, 2, or 3 h). Upin the completion of reaction time, 5 mL of n-hexane and 5 mL of distilled water were added to the products (biodiesel and glycerol), giving rise to two distinct phases which were separated from each other using a separating funnel. The catalyst and glycerol were dispersed in the water phase (the lower phase) while the biodiesel was dispersed in the n-hexane phase (the upper phase). Biodiesel was recovered from the mixture with n-hexane by heating until n-hexane was evaporated. The catalyst was then regenerated by filtering the products in the water phase, followed by drying. The yield of biodiesel was calculated using **Equation 3**;

$$Yield(\%) = \frac{Weight\ of\ biodiesel}{Weight\ of\ oil} \times 100 \quad \text{(Eq. 3)}$$

Please cite this article as: Aderibigbe F.A., Mustapha S.I., Adewoye T.L., Mohammed I.A., Gbadegesin A.B., Niyi F.E., Olowu O.I., Soretire A.G., Saka H.B. Qualitative role of heterogeneous catalysts in biodiesel production from *Jatropha curcas* oil. Biofuel Research Journal 26 (2020) 1159-1169. DOI: 10.18331/BRJ2020.7.2.4

2.2.5. Properties of biodiesel

The quality of the produced biodiesel was investigated by determining its physicochemical properties such as flash point, density, and viscosity. It was also characterized by using Gas Chromatography-Mass Spectroscopy (GC-MS) to investigate functional groups present, as well as the geometry and spatial isomerism of the produced biodiesel. An Agilent 7890A gas chromatograph (USA) hyphenated to a 5975C mass spectrophotometer with triple axis detector equipped with an auto-injector (10 µL syringe) was used. Helium was used as carrier gas. All chromatographic separation was performed on a capillary column having the following specifications: length; 30 m, internal diameter 0.2 µm, thickness; 250 µm, and treated with phenyl methyl silox. Other GC-MS conditions included ion-source temperature: 250 ºC, interface temperature: 300 ºC, pressure: 0.1117 MPa, out time: 1.8 mm, 1µl injector in split mode with the split ratio of 1:50 and with an injection temperature of 300 ºC. The column temperature was set at 35 ºC for 5 min and was elevated to 150 ºC at the rate of 4 ºC/min, the temperature was the raised again to 250 ºC at the rate of 20 ºC/min and held for 5 min. The total elution was 47.5 min. MS solution software provided by the manufacturer was used to control the system and to acquire data. Identification of the compounds was carried out by comparing the mass spectra obtained with those of the standard mass spectra from the NIST library (NIST11).

3. Results and Discussion

3.1. Leave extracts and formation of colloidal nanoparticles

3.1.1. Amaranthus spinosus extract and colloidal MgO

The FTIR spectrum of *A. spinosus* leaf extract is presented in **Figure S2**, showing characteristic bands for several functional groups. The spectrum analysis confirmed the presence of amaranthine and phenolic compounds, functional groups in the leave extract. The absorption band at 3445.91 cm^{-1} implies the presence of strong OH as well as NH stretching of phenol and amine group. The presence of carbonyl functional group around 1631.66 cm^{-1}, C–O group around 1159.89 cm^{-1}, and >C=O at about 1064.91 cm^{-1} are also observed. The result obtained agrees in part with those of the previous works by Das et al. (2012) and Muthukumar and Matheswaran (2015) who also observed hydroxyl, aromatic amines, aliphatic amines, carbonyl, C–H, and C=C (benzene) functional groups.

Being effective reducing and capping agents, the presence of these groups in the leaf extract assisted with the formation of nanoparticles from the precursor solution. Presented in the **Figure S1** is the UV-Vis spectrum of the colloidal MgO nanoparticles that were formed by using the green synthesis route.

The solution containing the MgO nanoparticles was analyzed using a UV-Vis spectrophotometer to confirm the formation of the particles. The resulting absorbance peak at 330 nm confirmed the successful formation of the MgO nanoparticles.

3.1.2. Extract of Citrus aurantifolia and colloidal ZnO

Figure S3 shows the FTIR spectrum of *C. aurantifolia* leaf extract. The band at 570.98 cm^{-1} is associated to the CH_2 group deformation. The C–O of aliphatic acid groups are attributed to the peak from 1216.89 cm^{-1}. The medium strong band at 1641.16 cm^{-1} is assigned to the deformation C–OH of carboxyl. The intense absorption peak around 3493.40 cm^{-1} indicates the existence of free and intermolecular bonded hydroxyl groups. The OH stretching vibrations occur within a broad range of frequencies indicating the presence of "free" hydroxyl groups and bonded OH groups of carboxylic acids (Andronie et al., 2017). The presence of these compounds suggests that the leaf extract is a suitable reducing agent that could effectively precipitate out the zinc oxide from the zinc nitrate precursor.

3.2. Characterization of catalysts

3.2.1. Crystalline nature of the catalysts

The XRD patterns of the catalysts prepared by the green synthesis and wet impregnation methods were acquired and are presented in **Figures 1a-d**. All catalyst samples were shown to be crystalline, forming complex metal oxides of the metals involved. The identified peaks of MgO and ZnO shown in **Figures 1b** and **1d** reveal that the nitrate salts of magnesium and zinc which were used as starting materials during the green synthesis method were adequately reduced to their respective oxides by the leave extracts of *A. spinosus* and *C. aurantifolia*, respectively. In **Figure 1a**, the MgO is seen to exhibit four peaks at 2θ angles of 37.0°, 42.8º, 62.3°, and 78.5° mainly due to MgO – periclase (JCPDS card No.00-045-0946).

In the XRD pattern of green synthesized *Fe-Co-Ni-MgO* shown in **Figure 1b**, the peaks at 35.5°, 44.0°, 43.0°, 62.3°, and 78.6° represent majorly $MgFe_2O_4$ phase – magnesioferrite (JCPDS card No.00-036-0398). Some other peaks representing MgO – periclase (JCPDS card No. 00-045-0946) were also observed.

The XRD analysis of the wet impregnation–prepared *Fe-Co-Ni/ZnO* catalyst is presented in **Figure 1c**. The major peaks at 31.7º, 34.5º, 36.2º, 47.5º, 56.6º, 62.9 º, 66.3º, 67.9º, 69.1º, 72.5º, and 76.9º indicate the presence of ZnO – zincite (JCPDS card No. 00-036-1451). At 43.3º, a small peak confirms the presence of NiO (JCPDS card No.00-047-1049). The sharpest peak occurring at 36.2º denotes the ZnO present in the nanocatalyst which is highly crystalline. In **Figure 1d**, the XRD pattern of the green synthesized *Fe-Co-Ni-ZnO* is presented. In addition to the highly crystalline nature, very similar result was obtained compared to the XRD pattern of *Fe-Co-Ni/ZnO* catalyst prepared by the wet impregnation method (**Fig. 1c**).

Moreover, major peaks at 2θ angles of 31.8, 34.4, 36.3, 47.5, 56.6, 62.9, 67.9, and 72.5° were identified, showing the presence of ZnO – zincite (JCPDS card No. 00-036-1451). The peak at 34.4° indicates the presence of NiO. The peaks corresponding to individual metallic particles (Fe, Co, or Ni) were not detected possibly due to their low concentrations in the mixture.

3.2.2. Morphological characteristics of the catalysts

Despite similar starting materials used as precursors in their preparation, the four catalysts exhibited distinct morphologies due to their different methods of synthesis.

(a) The SEM analysis of Fe-Co-Ni/MgO catalyst

High resolution SEM images of the *Fe-Co-Ni/MgO* catalyst are shown in **Figures 2a-d**. The SEM was used to investigate the morphological characteristics of the catalyst and the extent of deposition of the active metals on the support. As shown in **Figure 2a**, the SEM result at 100 nm scale depicts clustered solid catalyst material that is crystalline, in which particles are near-spherical in geometry. Agglomerates seen in the SEM image could have formed from the drying process during sample preparation. The material is observed to exhibit micro-porous structure (**Figs. 2c** and **d**); lower magnification images at 1µm and 10µm). Homogeneous appearance of the material's surface is indicative that Fe, Co and Ni nanoparticles were properly dispersed on the MgO support material.

(b) The SEM analysis of Fe-Co-Ni-MgO catalyst

Figures 3a-d present the SEM results of the green-synthesized *Fe-Co-Ni-MgO* catalyst, showing a regular structure which is well defined with smaller nanosized particles dispersed over its surface (**Figs. 3a** and **b**). The regular structure is presumably that of MgO caused by combined chemical effect and thermal treatment. While **Figures 3a** and **3b** show clearly the deposition of smaller crystals of Fe, Co, and Ni onto the larger MgO particles. These images (**Figs. 3a** and **b**) also suggest that the larger tetrahedron particles be in the order of microns. An approximate estimation of the size of the nanoparticles dispersed on the surfaces is in the sub-100 nm range. In **Figure 3d** which depicts the catalyst material in clusters, the catalyst is shown to be porous and should therefore have abundant active reaction sites.

(c) The SEM analysis of Fe-Co-Ni/ZnO catalyst

Presented in **Figures 4a-d** are the SEM images of the *Fe-Co-Ni/ZnO* catalyst synthesized by wet impregnation. The small nanoparticles of Fe,

Please cite this article as: Aderibigbe F.A., Mustapha S.I., Adewoye T.L., Mohammed I.A., Gbadegesin A.B., Niyi F.E., Olowu O.I., Soretire A.G., Saka H.B. Qualitative role of heterogeneous catalysts in biodiesel production from *Jatropha curcas* oil. Biofuel Research Journal 26 (2020) 1159-1169. DOI: 10.18331/BRJ2020.7.2.4

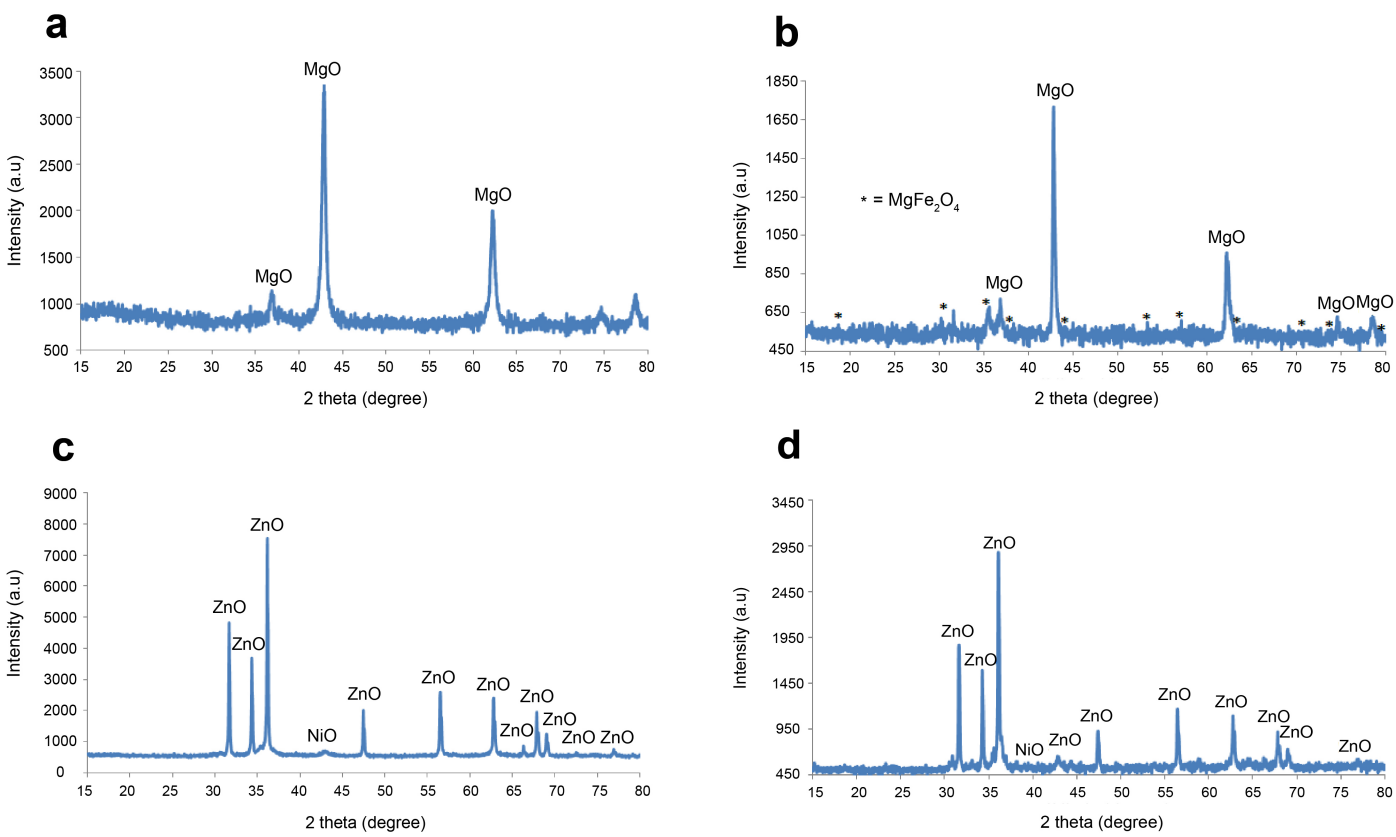


Fig. 1. XRD pattern of (a) *Fe-Co-Ni/MgO* catalyst prepared by wet impregnation, (b) *Fe-Co-Ni-MgO* catalyst prepared by green synthesis, (c) *Fe-Co-Ni/ZnO* catalyst prepared by wet impregnation, and (d) *Fe-Co-Ni-ZnO* catalyst prepared by green synthesis.

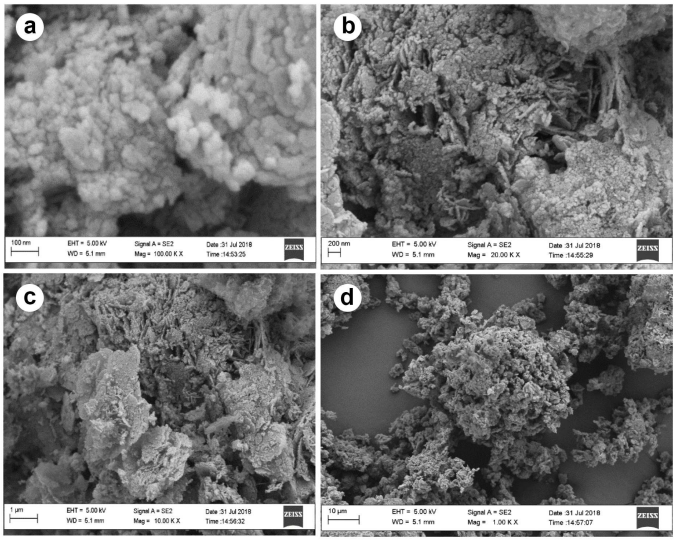


Fig. 2. High resolution SEM image of the *Fe-Co-Ni/MgO* catalyst obtained at different scales of (a) 100 nm, (b) 200 nm, (c) 1 µm, and (d) 10 µm.

Co, and Ni, and the ZnO support material can be observed. The SEM images shown in **Figures 4a** and **4b** represent three dimensional particles of near-spherical shape that are highly crystalline. The high crystallinity is in agreement with the XRD result presented earlier in **Figure 1**. The deposition of iron, cobalt, and nickel nanoparticles on the zinc oxide support is clearly seen as represented by particles in the sub-20 nm size range. In **Figures 4c** and **4d**,

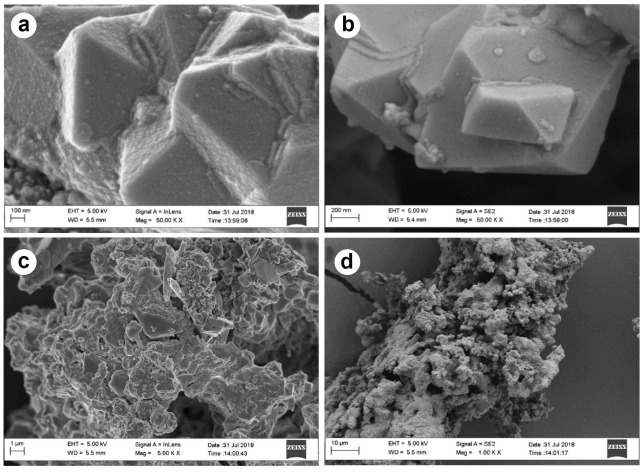


Fig. 3. High resolution SEM image of the *Fe-Co-Ni-MgO* catalyst obtained at different scales of (a) 100 nm, (b) 200 nm, (c) 1µm, and (d) 10µm.

small micro-pores could be identified. It was also revealed that there was an even dispersion/distribution of the metals onto the ZnO support material.

(d) The SEM analysis of Fe-Co-Ni-ZnO catalyst

In the catalysts prepared by the wet impregnation method, phase distinction between the deposited active components and the support

Please cite this article as: Aderibigbe F.A., Mustapha S.I., Adewoye T.L., Mohammed I.A., Gbadegesin A.B., Niyi F.E., Olowu O.I., Soretire A.G., Saka H.B. Qualitative role of heterogeneous catalysts in biodiesel production from *Jatropha curcas* oil. Biofuel Research Journal 26 (2020) 1159-1169. DOI: 10.18331/BRJ2020.7.2.4

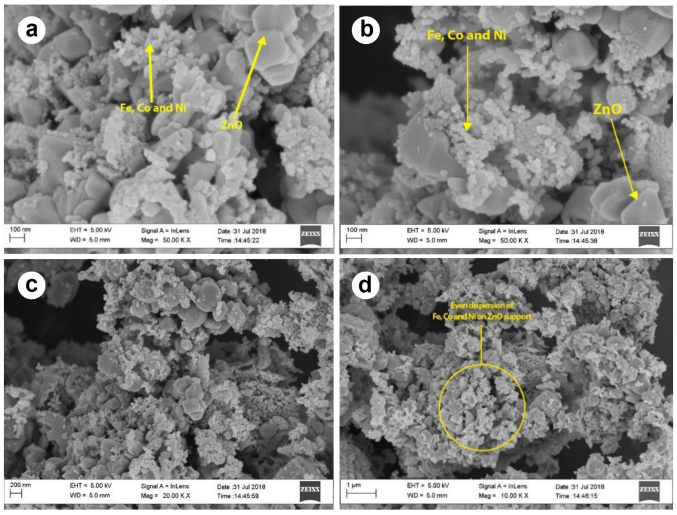


Fig. 4. High resolution SEM images of the *Fe-Co-Ni/ZnO* catalyst at different scales of (a,b) 100 nm, (c) 200 nm, and (d) 1µm.

material could be observed (Figs. 2 and 4). In contrast, the catalysts prepared by the green synthesis method appeared bespoke (Figs. 3 and 5). The *Fe-Co-Ni-ZnO* catalyst synthesized by the green synthesis route, as shown in Figures 5a-d, exhibited regular near-spherical structures with a narrow particle size distribution (Figs. 5a and 5b), which are characteristics of bespoke green nanomaterials. All the nanoparticles were within the sub-10 nm particle size range, with some agglomerated to form bigger particle clusters (Fig. 5b). Similar to the morphology difference observed between the *Fe-Co-Ni/MgO* and *Fe-Co-Ni-MgO* catalysts prepared by the wet impregnation and green synthesis methods, the *Fe-Co-Ni-ZnO* catalyst obtained through the green synthesis route also showed a morphology that was different from its wet impregnation counterpart. Moreover, the solid catalyst material was highly crystalline (Figs. 5c and d), which was also evident from the related XRD results (Fig. 1d). Micropores could also be identified in the catalyst composite.

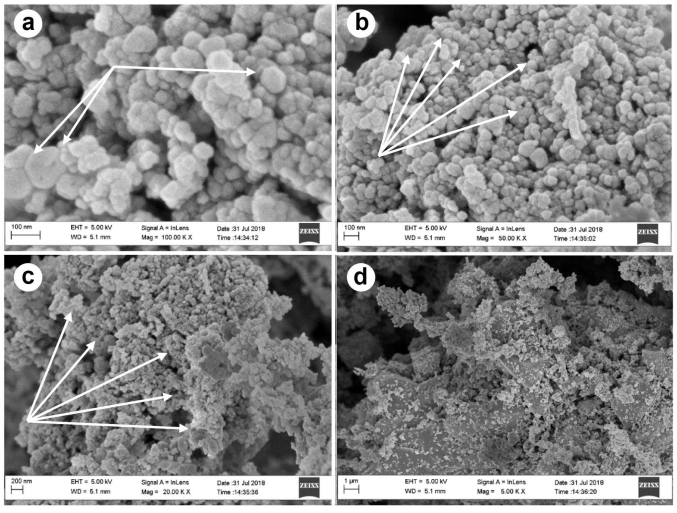


Fig. 5. High resolution SEM images showing *Fe-Co-Ni-ZnO* catalyst at different scales of (a) 100 nm, (b) 100nm, (c) 200nm, and (d) 1 µm.

3.2.3. Elemental composition

In the EDS qualitative and quantitative elemental analyses of all the four catalysts, metallic Fe, Co, Ni, Mg, and Zn were found. Based on the EDS results, the presence of the Fe, Co, Ni, Mg, and Zn metals around the line energy position of oxygen indicate the formation of complex oxides of these metals with oxygen. The EDS elemental analysis also showed that carbon is present in all the samples because carbon was used as the coating material during the EDS analysis. Carbon is the recommended coating materials as it does not interfere with the characteristics X-ray peaks from elements in samples. The EDS results are presented in Figure S4.

In the qualitative EDS result of the *Fe-Co-Ni/MgO* catalyst presented in Figure S4a, the elemental composition in the catalyst was found as (in atomic %): C (12.71), O(46.64), Mg(35.45), Fe(1.55), Co(1.05), and Ni (2.61).

The EDS of the green synthesized *Fe-Co-Ni-MgO* catalyst (Fig. S4b) presented atomic % elemental composition of C(12.74), O(36.54), Mg(33.11), Cl(4.56), K(0.24), Fe(3.15), Co(3.49), and Ni(6.17). Obviously, Mg, O, Fe, Co, and Ni were introduced by the precursor salts, while Cl and K were from the leaf extract. In this case, carbon could be from the plant extract or coating material used during sample preparation for the EDS analysis.

The *Fe-Co-Ni/ZnO* catalyst prepared by wet impregnation presented EDS elemental composition of C(29.22), O(28.17), Na(6.33), Fe(3.62), Co(1.4), Ni(2.85), and Zn(28.4) (in atomic %). Again, carbon was introduced from the coating material during the EDS sample preparation stage, and Na was an impurity. The presence of oxygen is indicative of formation of complex oxides of the Fe, Co, Ni, and Zn metals. These components are were found in the qualitative EDS result shown in Figure S4c.

In Figure S4d, the qualitative EDS result of the green-synthesized *Fe-Co-Ni-ZnO* catalyst is presented. Its atomic % elemental composition was found as C(19.65), O(36.13), K(0.46), Fe(6.74), Co(7.98), Ni(12.4), and Zn(16.64). The composition of *Fe-Co-Ni-ZnO* significantly differed from that of *Fe-Co-Ni/ZnO*, thus implying potentially different catalytic activity. Based on the EDS results, oxides of Fe, Co, Ni, and Zn might have been formed. Carbon could be from the leaf extract or EDS coating material as mentioned earlier. The metals Fe, Co, and Ni are from the salt precursor while K might have been introduced by the leaf extract.

3.2.4. Thermal stability

The thermal behavior of the prepared catalysts was investigated using the TGA/DSC analyses over a temperature range of up to 900°C at the rate of 10°C min^{-1} under nitrogen atmosphere. Accordingly, the catalysts prepared by the wet impregnation technique were found to be more thermally stable than their equivalent ones prepared by the green synthesis method.

Figure 6a reveals that the *Fe-Co-Ni/MgO* catalyst was thermally stable, losing only about 6 wt% of its original weight by rising the temperature up to 900°C. A two-step thermal degradation and weight loss was first observed; at 100–200°C, and 220–320°C. The first weight loss could represent the loss of absorbed moisture while the second might be ascribed to the elimination of the crystal water. But a weight gain regime was also observed which occurred at above 550°C. The initiation of a third weight loss regime above 300°C could be attributed to the decomposition of magnesium oxide while the subsequent weight gain could be indicative of phase transformation, involving the formation of new compound(s) – $Mg(OH)_2$.

In the TGA/DSC curves of *Fe-Co-Ni-MgO* (Fig. 6b), there are several regimes of weight loss which is typical of a mixture of many components exhibiting their individual thermal degradation. As one would expect, the leaf extract contained several phytochemicals and must have presumably introduced these to the catalyst material, possibly by forming complexes with the Fe, Co, Ni, and Mg metal cations or their oxides. Throughout the heating up to 800°C, this catalyst lost about 12 wt% of its initial weight. Of these, about 7 wt% was lost below 220°C which could be attributed to several volatile compounds from the green source. Apart from the weight loss prior to 220°C, a weight loss was observed at 300–550°C, and another at 720–820°C. Some decomposition also occurred in this material thereby changing its thermal degradation behavior; the latter two regimes could be attributed to the degradation of individual components which could be complex compounds that had formed. Agglomeration and grain growth forming large crystalline structures with sizes in microns was also observed in the high resolution SEM images of this sample (Fig. 3).

Please cite this article as: Aderibigbe F.A., Mustapha S.I., Adewoye T.L., Mohammed I.A., Gbadegesin A.B., Niyi F.E., Olowu O.I., Soretire A.G., Saka H.B. Qualitative role of heterogeneous catalysts in biodiesel production from *Jatropha curcas* oil. Biofuel Research Journal 26 (2020) 1159-1169. DOI: 10.18331/BRJ2020.7.2.4

Overall, given their total weight loss percentages at above 800°C, *Fe-Co-Ni/MgO* could be regarded as more thermally stable compared with *Fe-Co-Ni-MgO*.

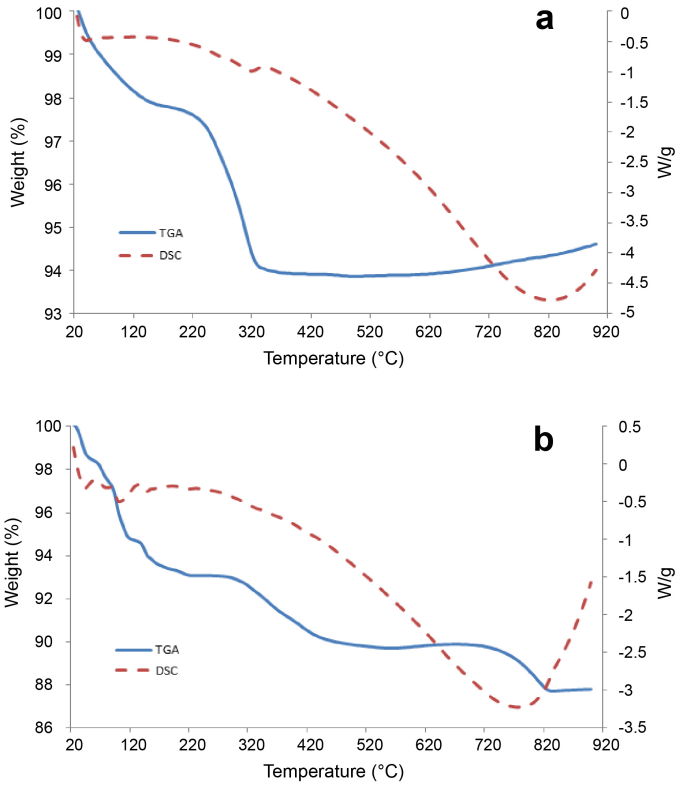


Fig. 6. TGA/DSC of (a) *Fe-Co-Ni/MgO* catalyst (wet impregnation method), and (b) *Fe-Co-Ni-MgO* catalyst (green synthesis method).

3.2.5. Functional groups

Remarkable observation can be made from the FTIR spectra of the catalysts, comparing *Fe-Co-Ni/MgO* with *Fe-Co-Ni-MgO*, and *Fe-Co-Ni/ZnO* with *Fe-Co-Ni-ZnO*. The pairs show similar FTIR spectra which further prove that their compositions, i.e., their surface functional groups, are at large alike. For instance, the spectra of *Fe-Co-Ni/MgO* and *Fe-Co-Ni-MgO* as presented in **Figures S5** and **S6** respectively, share broad and narrow bands, stretches, and vibrations at similar wavelengths.

In the FTIR spectrum of *Fe-Co-Ni/MgO* presented in **Figure S5**, the medium peaks at 3699.21 cm^{-1} and 3458.58 cm^{-1} are the result of stretching O-H bonded to the surface of solids derived from adjacent water molecules (Andronie et al., 2017; Sutapa et al., 2018). The medium peak at 1670.35 cm^{-1} could derive from the asymmetric vibrations (vas) of C–O in Mg-oxalate complex, and the peak at 1381.53 cm^{-1} could be assigned to the symmetry vibration (vs) C–O and δ(O–C–O) (Sutapa et al., 2018).

The FTIR spectrum of *Fe-Co-Ni-MgO* catalyst presented in **Figure S6** shows major absorption bands occurring at 3654.88, 3632.72, 3449.08, 3325.59, 1625.33, 1435.36, and 577.31 cm^{-1} which could be attributed to the asymmetric stretches, out of plane bends and in-plane bend vibration modes. These denote free and bonded alcohols and phenols (O–H stretch), nitramines (NO_2 stretch), alkanes/alkyl groups, alkenes (C=C–H in plane bends), and alkynes (C–H bend), indicating that the functional groups such as flavones must have been transformed whilst acting as reducing and capping agents in the nanoparticle formation. Various other minor absorption bands occurred at 2898.15, 2828.50, 1530.34, 1476.52, 1349.87, 1302.37, and 830.61 cm^{-1} which could be assigned to alkanes (methyl, methylene, and methane) (C–H stretch), aromatic (2 or 3 bends only) (C=C stretch), alkenes/alkyl groups, aromatics, and meta-distributed benzene (C–H deformed vibrations).

Similarly, the spectra of *Fe-Co-Ni/ZnO* and *Fe-Co-Ni-ZnO* presented in **Figures S7** and **S8** were observed to share bands, stretches, and vibrations at the same wavelengths. In **Figure S7**, the absorption band at 3474.41 cm^{-1} indicates the presence of –OH hydroxyl groups. The 1615.83 cm^{-1} absorption band reveals the presence of –C=O functional group stretching deformation and that at 992.08 cm^{-1} suggests the presence of –C–O– stretching deformation. The presence of C–H functional group deforming vibration is represented by the peaks at 1492.35cm^{-1} and 881.27cm^{-1}, while the presence of C–N stretching vibration is indicated by the band recorded at 1356.20cm^{-1}.

The FTIR spectrum of the green-synthesized *Fe-Co-Ni-ZnO* shown in **Figure S8** reveals the presence of aromatics and alkanes/alkyl groups. The absorption bands at 1587.34 cm^{-1} and 1558.84 cm^{-1} indicate the presence of C=C functional groups. The absorption bands at 1482.85cm^{-1}, 1448.02 cm^{-1}, and 1381.53 cm^{-1} represent the presence of C–H deforming vibration. Generally, despite the observed similarities in their functional groups, the participation of each pair of the four catalysts in the transesterification reaction may not present similar activities because of the influences of the other structural factors of the catalytic materials.

3.3. Optimization of biodiesel production

The performance of the four synthesized catalysts in the transesterification reaction was investigated by varying reaction parameters in a Box-Behnken Design (BBD) of experiment as tabulated in **Table 1**. Each experiment had 27 experimental runs and the optimum value was identified in each case. The summary of the BBD experimental results is presented in **Table 2**.

Table 2.
Summary of the BBD experimental results for biodiesel production using the four investigated catalysts.

S/N	Catalyst	Synthesis method	Optimum yield (%)	Optimum conditions
1	*Fe-Co-Ni/MgO*	Wet impregnation	92.2	MeOH: oil ratio (15:1 w/w), Catalyst (15%, w/w), at 55°C and 1 h.
2	*Fe-Co-Ni-MgO*	Green synthesis	97.9	MeOH: oil ratio (15:1 w/w), Catalyst (15% w/w), at 55°C and 1 h.
3	*Fe-Co-Ni/ZnO*	Wet impregnation	86.6	MeOH: oil ratio (10:1 w/w), Catalyst (10% w/w), at 60°C and 1 h.
4	*Fe-Co-Ni-ZnO*	Green synthesis	91.4	MeOH: oil ratio (15:1 w/w), Catalyst (5% w/w), at 55°C and 3 h.

The ANOVA for these experiments was used to generate regression models which are represented in **Equations 4-7**. The regression models show how the four reaction parameters; i.e., MeOH:oil molar ratio, temperature, time, and catalyst concentration, influenced biodiesel yield when each catalyst was employed.

$$Y_{Fe-Co-Ni/MgO} = -2268.82 + 42.84A + 72.20B + 60.28C - 6.92D - 0.348AB - 1.855AC - 0.307AD + 0.245BD - 0.87CD - 0.545A^2 - 0.623B^2 - 8.05C^2$$

(Eq. 4)

$$Y_{Fe-Co-Ni-MgO} = -2894.69 + 18.25A + 100.10B + 26.96C - 6.90D - 0.21AB - 1.08AC - 0.413AD + 0.28BD - 1.585CD - 0.88B^2$$

(Eq. 5)

$$Y_{Fe-Co-Ni/ZnO} = -1622.69 + 17.44A + 61.0B - 75.63C - 4.16D - 0.39AB + 1.45AC + 0.478AD - 0.08BC + 1.455CD - 0.13A^2 - 0.52B^2 + 8.95C^2 - 0.26D^2$$

(Eq. 6)

Please cite this article as: Aderibigbe F.A., Mustapha S.I., Adewoye T.L., Mohammed I.A., Gbadegesin A.B., Niyi F.E., Olowu O.I., Soretire A.G., Saka H.B. Qualitative role of heterogeneous catalysts in biodiesel production from *Jatropha curcas* oil. Biofuel Research Journal 26 (2020) 1159-1169. DOI: 10.18331/BRJ2020.7.2.4

$$Y_{Fe-Co-Ni-ZnO} = -2147.98 - 15.4A + 69.8B + 197.38C - 48.1D + 0.564AB - 0.285AC - 0.38AD - 2.78BC - 0.693BD - 1.915CD - 0.37A^2 - 0.6B^2 - 6.28C^2 - 0.147D^2 \quad \text{(Eq. 7)}$$

where A is MeOH:oil molar ratio, B stands for temperature (°C), C is time (h), and D denotes catalyst concentration. The model equations were reliable, showing significant (<0.05) model *p*-values of 0.0456, 0.0094, 0.0367, and 0.0390 in **Equations 4**, **5**, **6**, and **7**, respectively. The highest biodiesel yield of 97.9% was obtained with the green-synthesized *Fe-Co-Ni-MgO* catalyst. It was also observed that both catalysts based on MgO support exhibited relatively higher catalytic performance compared to their ZnO-based counterparts.

3.4. Physicochemical properties and FAME profiles

The FAME profiles of the *J. curcas* oil-based biodiesel products and their physicochemical properties were investigated in order to establish the effect of catalyst type on the quality/composition of the produced biodiesel. A summary of the FAME profiles of biodiesel products produced by various catalysts are presented in **Table 3**. As shown in **Table 3**, the biodiesel samples showed a total saturated fatty acid of 2.94–21.73% and total unsaturated fatty acid of 78.27–97.06%. The high degree of unsaturation is typical feature of Jatropha of Jatropha biodiesel produced using the four catalysts are presented in **Figures S9-12**.

The Jatropha biodiesel obtained using the green-synthesized *Fe-Co-Ni-MgO* contained unsaturated acid of oleic acid (78.27 wt%), and saturated acids of n-hexadecanoic acid (12.14 wt%), octadecanoic acid (6.87 wt%), cyclohexanecarboxylic acid, undecyl ester (2.72 wt%). The total percentage composition of FAMEs was greater than the minimum FAME requirement of 96.5% specified by the ASTM (**Fig. 7**). Overall, the product produced by *Fe-Co-Ni-MgO* catalyst consisted of 78.27% unsaturated and 21.73% saturated fatty acids (**Fig. 8**). Hence, the biodiesel obtained using this green-synthesized catalyst resulted in the highest yield and the lowest degree of unsaturation in spite of the fact that high degree of unsaturation is a general characteristic of Jatropha biodiesels (Mofijur et al., 2017).

The Jatropha biodiesel produced from the wet impregnation-prepared *Fe-Co-Ni/ZnO* catalyst consisted of 88.9% unsaturated and 11.1% saturated fatty acids (**Fig. 8**). This indicates that the catalyst produced a low-grade biodiesel, since the higher the percentage of unsaturated fatty acids in biodiesel, the lower its oxidative and thermal stability would be. In another words, this denotes that the resultant biodiesel would deteriorate faster in high-temperature environments. The biodiesel produced by green-synthesized *Fe-Co-Ni-ZnO* catalyst contained 8.74 wt% n-haxadacanoic acid, 81.4 wt% oleic acid, 7.71 wt% octadecanoic acid, and 2.51 wt%

Table 3.
FAME compositions of the biodiesel products by various catalysts.

Catalyst	RT[a]	Methyl ester	Molecular formula	Composition (%)
Fe-Co-Ni/MgO (Wet Impregnation)	38.737	Oleic acid, 9-Octadecenoic acid, cis-Vaccenic acid	$C_{19}H_{36}O_2$	97.06
	43.959	Cyclohexanecarboxylic acid, pentadecyl ester; Docosanoic acid,4,4-dimethyl-ester; Adipic acid,butyl 2-pentylester	$C_{22}H_{42}O_2$	2.94
Fe-Co-Ni-MgO (Green Synthesis)	35.555	n-Hexadecanoic acid AN[d]: palmitic acid	$C_{16}H_{32}O_2$ (Sat.[b])	12.14
	39.037	6-Octadecanoic acid, 9-Octadecanoic acid, (E) - Oleic acid	$C_{18}H_{34}O_2$ (Unsat.[c])	78.27
	39.276	Octadecanoic acid AN: Stearic acid	$C_{17}H_{35}COOH$ (Sat.)	6.87
	43.971	Cyclohexanecarboxylic acid, undecyl ester; Cyclohexanecarboxylic acid, heptyl ester; Adipic acid, butyl 2-pentyl ester AN: Undecyl cyclohexanecarboxylate	$C_{18}H_{34}O_2$ (Sat.)	2.72
Fe-Co-Ni/ZnO (Wet Impregnation)	20.872	Cyclohexasiloxane, dodecamethyl-cyclohexasiloxane, dodecamethyl-5-[4-(Dimethylamino) benzylideneamino]-2-phenyl-2H-benzotriazole	$C_{12}H_{36}O_6Si_6$ (Sat.)	3.32
	25.221	N-benzyl-N-ethyl-p-isopropylbenzamide, pentasiloxane, dodecamethyl-4H-1,2,4-Triazole-3-thiol, 4-allyl-5-(1-naphthylmethyl)-	$C_{19}H_{23}NO$ (Unsat.)	8.25
	29.115	Silane,[[4-[1,2-bis[(trimethylsilyl)oxy]ethyl]-1,2-phenylene]bis(oxy)]bis[trimethyl- Silane,[[4-[1,2-bis[(trimethylsilyl)oxy]ethyl]-1,2-phenylene]bis(oxy]bis[trimethyl- Cyclopentasiloxane, decamethyl	$C_{10}H_{30}Si_5$ (Sat.)	4.77
	36.979	13-Hexyloxacyclotridec-10-en-2-one Bicylco[2.2.1] heptan-2-one, 3-(2-oxopropyl)-, exo- Bicylco(5.3.1) undecan-11-one	$C_{11}H_{18}O$ (Sat.)	3.01
	37.697	9-octadecenoic acid (Z)-, methyl ester 15-octadecenoic acid, methyl ester 9-octadecenoic acid, methyl ester	$C_{18}H_{34}O_2$ (Unsat.)	3.06
	38.648	cis-13-octadecenoic acid cis-vaccenic acid 9,12-octadacadienoic acid(z,z)	$C_{18}H_{34}O_2$ (Unsat.)	77.59
Fe-Co-Ni-ZnO (Green Synthesis)	35.489	n-Hexadecanoic acid	$C_{16}H_{32}O_2$	8.74
	38.982	Oleic acid 6-octadecanoic acid 9-octadecanoic acid	$C_{18}H_{34}O_2$	81.04
	39.221	Octadecanoic acid	$C_{18}H_{36}O_2$	7.71
	43.960	Cyclohexanecarboxylic acid, undecyl ester	$C_{15}H_{28}O_2$	2.51

[a] RT: Retention time; [b] Sat.: Saturated; [c] Unsat.: Unsaturated; [d] AN: Another name

Please cite this article as: Aderibigbe F.A., Mustapha S.I., Adewoye T.L., Mohammed I.A., Gbadegesin A.B., Niyi F.E., Olowu O.I., Soretire A.G., Saka H.B. Qualitative role of heterogeneous catalysts in biodiesel production from *Jatropha curcas* oil. Biofuel Research Journal 26 (2020) 1159-1169. DOI: 10.18331/BRJ2020.7.2.4

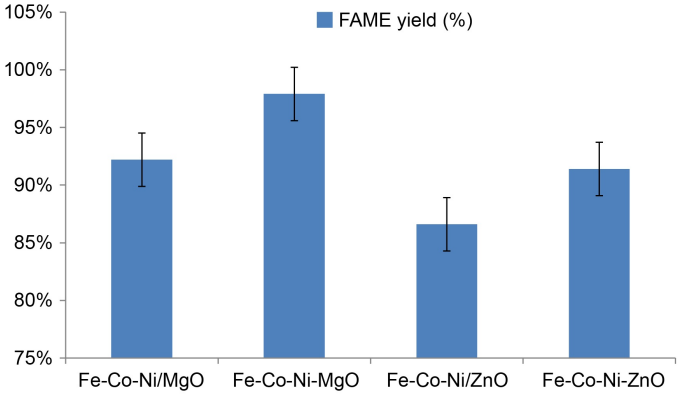


Fig. 7. FAME yield (%) of the four catalysts used.

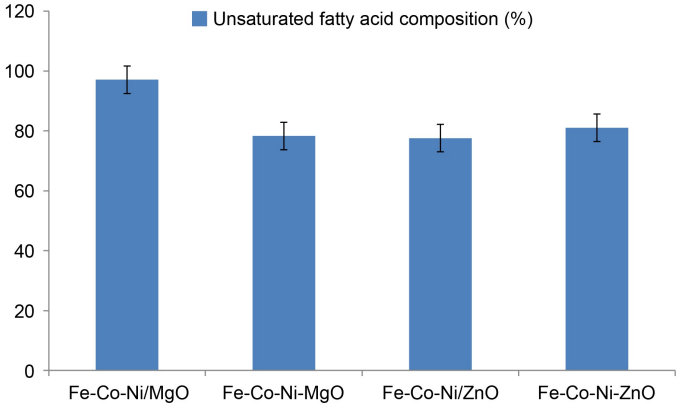


Fig. 8. The composition of unsaturated fatty acids in the biodiesels produced using the four catalysts.

cyclohexanecarboxylic acid undecyl ester (Fig. 8). The maximum FAME conversion achieved using this catalyst stood at 81.04% (Fig. 7) with oleic acid as the most abundant FAME. Moreover, the FAME profile consisted of 81.04% unsaturated and 18.96% saturated fatty acids. Overall, apart from the major influence of Jatropha oil used as feedstock, the catalysts prepared either by the wet impregnation or green synthesis methods were shown to affect the FAME compositions of the final biodiesel products. It is however interesting to note that the combined influence of MgO as support material and the green synthesis route as catalyst preparation technique (i.e., using green-synthesized *Fe-Co-Ni-MgO* catalyst) resulted in the most favorable outcomes both quantitatively and qualitatively in comparison with the application of the three catalysts. A comparison of the highest FAME yield obtained in the current study (i.e., for *Fe-Co-Ni-MgO*) and those reported in the most recent literature is presented in Table 4.

Physicochemical properties of the biodiesels produced by the catalysts *vs.* the ASTM standard values are tabulated in Table 5 and Figure 9; confirming the acceptable quality of the products while also revealing considerable differences among them depending on the catalyst employed.

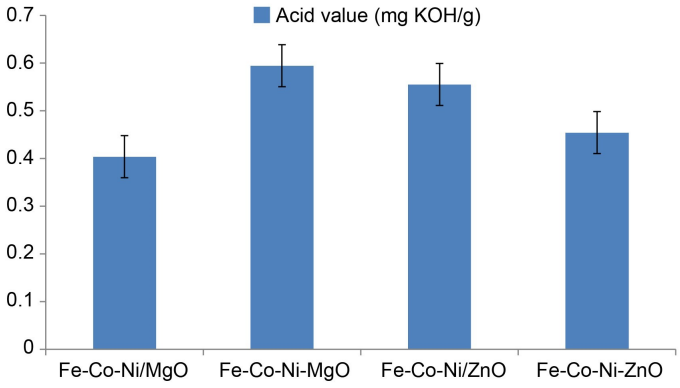
Table 4.
Comparison of the FAME yield of *Fe-Co-Ni-MgO* with the other solid catalysts used for biodiesel production reported in the literature.

S/N	Catalyst	Synthesis method	FAME Yield (%)	Reference
1	Magnetic core-shell SO_4/Mg-Al-Fe_3O_4	Stepwise co-precipitation, encapsulation, and surface functionalization	98.5	Gardy et al. (2019)
2	Mg/Al/Zn-based hydrotalcite/SBA-15	Rational design using a versatile *in situ* method including synthesis of macroporous hydrotalcite-derived oxides comprising ordered silica architectures	90	Prabu et al. (2019)
3	*Fe-Co-Ni-MgO*	Green synthesis	97.9	Present Study

Table 5.
Physicochemical properties of biodiesel produced by the four different catalysts, i.e., (a) *Fe-Co-Ni/MgO*, (b) *Fe-Co-Ni-MgO*, (c) *Fe-Co-Ni/ZnO*, and (d) *Fe-Co-Ni-ZnO*.

Fuel properties	(a)	(b)	(c)	(d)	ASTM standard
Density at 15 °C (g/cm^3)	0.882	0.8673	0.886	0.866	0.860 – 0.900 [1]
Kinematic viscosity at 40 °C (mm^2/s)	-	2.31	-	-	1.9 – 6.0 [2]
Flash point (°C)	198	142	209	219	≥130 [3]
Cloud point (°C)	-8	2	10	-2	-3 – 12 [4]
Pour point (°C)	2	-10	-4	-15	-15 – 10 [5]
Fire Point (°C)	193	148	223	230	≥130 [6]
Acid value (mg KOH/g)	0.4039	0.59466	0.5553	0.4544	≤0.80 [7]
FFA concentration (wt%)	-	0.5428	0.5069	0.4148	-

[1] ASTM D1298, [2] ASTM D445, [3] ASTM D92, [4] ASTM D2500, [5] ASTM D97, [6] ASTM D92, [7] ASTM D664



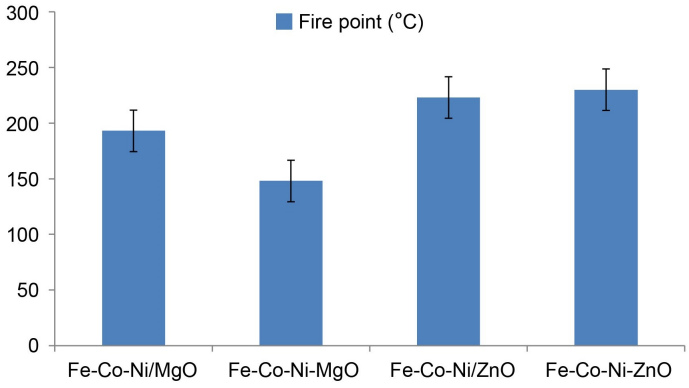


Fig. 9. The acid value, fire point, density at 15°C, flash point, FFA%, cloud point, and pour point of the biodiesels produced by using the different catalysts.

Please cite this article as: Aderibigbe F.A., Mustapha S.I., Adewoye T.L., Mohammed I.A., Gbadegesin A.B., Niyi F.E., Olowu O.I., Soretire A.G., Saka H.B. Qualitative role of heterogeneous catalysts in biodiesel production from *Jatropha curcas* oil. Biofuel Research Journal 26 (2020) 1159-1169. DOI: 10.18331/BRJ2020.7.2.4

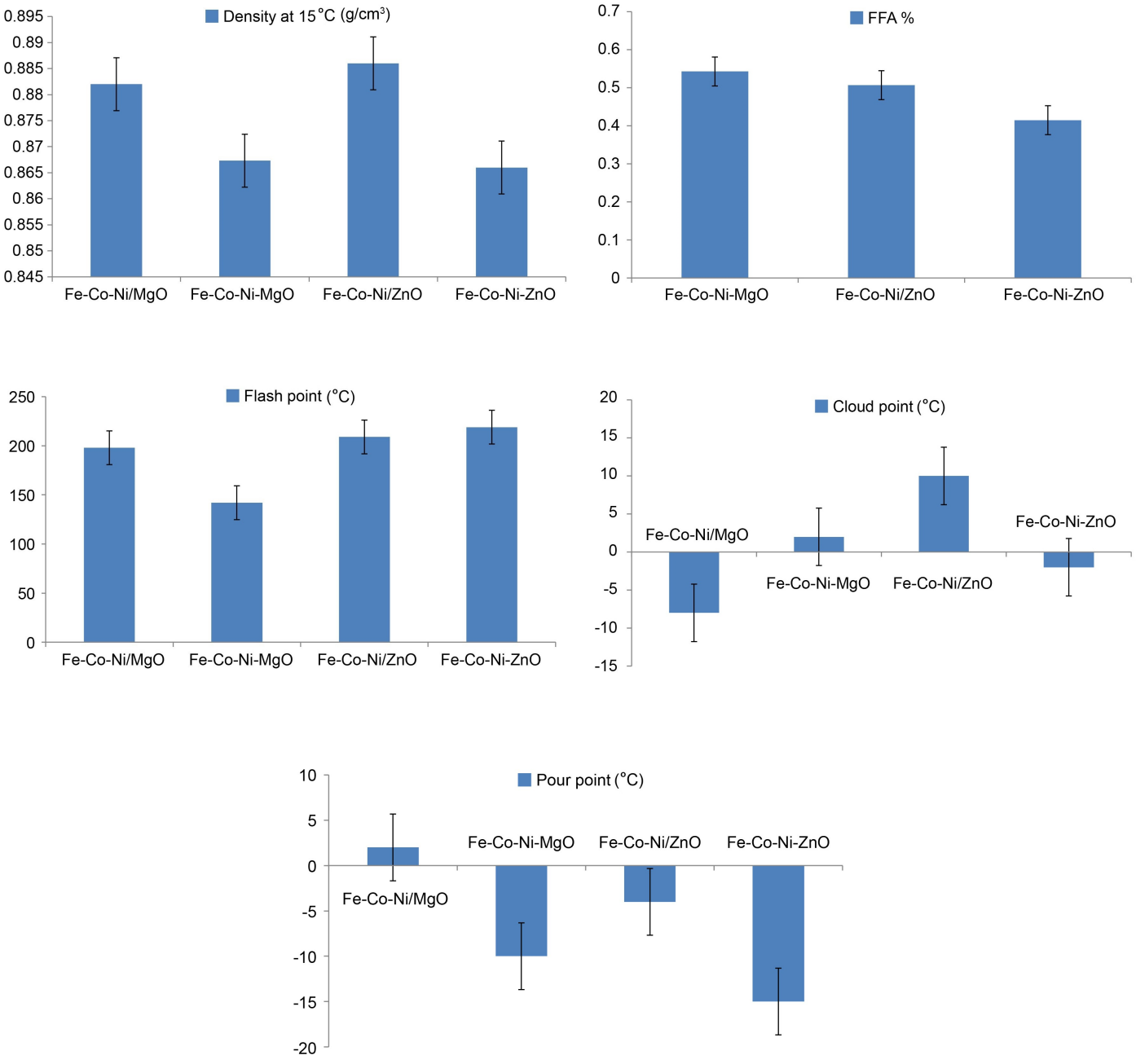


Fig. 9. continued.

4. Conclusions

The effects of green synthesis (using leaf extracts) and wet impregnation methods for the preparation of catalysts along with different support materials, on yield, composition, and properties of Jatropha biodiesel were investigated. As for the catalyst properties, the green-synthesized heterogeneous tri-metallic catalysts appeared more bespoke in morphology, but exhibited lower thermal stability. Irrespective of the method of synthesis, the crystalline phases revealed by the XRD and the FTIR spectra of the catalysts were dependent on the catalyst support material (MgO or ZnO). Moreover, the findings obtained revealed that catalyst type could determine FAME profile of the biodiesel produced from the same oil feedstock. More specifically, the support material used and the method employed for catalyst synthesis influenced the type of methyl esters found in the final biodiesel product. Higher yield was obtained with magnesium oxide as support material than with zinc oxide, and higher yields were obtained with green-synthesized catalysts

Please cite this article as: Aderibigbe F.A., Mustapha S.I., Adewoye T.L., Mohammed I.A., Gbadegesin A.B., Niyi F.E., Olowu O.I., Soretire A.G., Saka H.B. Qualitative role of heterogeneous catalysts in biodiesel production from *Jatropha curcas* oil. Biofuel Research Journal 26 (2020) 1159-1169. DOI: 10.18331/BRJ2020.7.2.4

compared with their counterparts synthesized through wet impregnation.

Acknowledgements

The authors wish to acknowledge the Department of Chemical Engineering, University of Ilorin, Nigeria, for permitting the use of laboratory facilities especially the GC-MS equipment.

References

[1] Abdulkareem, A.S., Kariim, I., Bankole, M.T., Tijani, J.O., Abodunrin, T.F., Olu, S.C., 2017. Synthesis and Characterization of tri-metallic Fe-Co-Ni catalyst supported on $CaCO_3$ for multi-walled carbon nanotubes growth via chemical vapor deposition technique. Arabian J. Sci. Eng. 42(10), 4365-4381.

[2] Al-Muhtaseb, A.H., Jamil, F., Al-Haj, L., Myint, M.T.Z., Mahmoud, E., Ahmad, M.N., Hasan, A.O., Rafiq, S., 2018. Biodiesel production over a catalyst prepared from biomass-derived waste date pits. Biotechnol. Rep. 20, e00284.

[3] Andronie, L., Coroiani, A., Miresani, V., Pop, I., Raducu, C., Odagiu, A., Marchuş, Z., Coroiani C., 2017. Vibrational study for the lemon and tangerine fruit using FT-IR spectroscopy. ProEnvironment /ProMediu. 10(31), 221-224.

[4] Altun S., 2014. Effect of the degree of unsaturation of biodiesel fuels on the exhaust emissions of a diesel power generator. Fuel. 117, 450-457.

[5] Banerjee, M., Dey, B., Talukdar, J., Kalita, M.C., 2014. Production of biodiesel from sunflower oil using highly catalytic bimetallic gold-silver core-shell nanoparticle. Energy. 69, 695-699.

[6] Benjumea, P., Agudelo, J.R., Agudelo, A.F., 2010. Effect of the degree of unsaturation of biodiesel fuels on engine performance, combustion characteristics, and emissions. Energy Fuels. 25(1), 77-85.

[7] Cruz-Ortiz, B.R., Ríos-González, L.J., 2017. Influence of the reaction parameters on biodiesel production catalyzed by a lipase from *Thermomyces lanuginosus* immobilized in PVA-alginate beads. Energy Sources Part A. 39(23), 2127-2132.

[8] Das, R.K., Gogoi, N., Babu, P.J., Sharma, P., Mahanta, C., Bora, U., 2012. The synthesis of gold nanoparticles using amaranthus spinosus leaf extract and study of their optical properties. Adv. Mater. Phys. Chem. 2(4), 275-281.

[9] De, S., Zhang, J., Luque, R., Yan, N., 2016. Ni-based bimetallic heterogeneous catalysts for energy and environmental applications. Energy Environ. Sci. 9(11), 3314-3347.

[10] Farooq, M., Ramli, A., Naeem, A., 2016. Effect of different metal oxides on the catalytic activity of γ-Al_2O_3-MgO supported bifunctional heterogeneous catalyst in biodiesel production from WCO. RSC Adv. 2016, 6(2), 872-881.

[11] Folayan, A.J., Anawe, P.A.L., Aladejare, A.E., Ayeni, A.O., 2019. Experimental investigation of the effect of fatty acids configuration, chain length, branching and degree of unsaturation on biodiesel fuel properties obtained from lauric oils, high-oleic and high-linoleic vegetable oil biomass. Energy Rep. 5, 793-806.

[12] Gardy, J., Nourafkan, E., Osatiashtiani, A., Lee, A.F., Wilson, K., Hassanpour, A., Lai, X., 2019. A core-shell SO_4/Mg-Al-Fe_3O_4 catalyst for biodiesel production. Appl. Catal., B. 259, 118093.

[13] Gardy, J., Osatiashtiani, A., Céspedes, O., Hassanpour, A., Lai, X., Lee, A.F., Wilson, K., Rehan, M., 2010. A magnetically separable SO_4/Fe-Al-TiO_2 solid acid catalyst for biodiesel production from waste cooking oil. Appl. Catal., B. 234, 268-278.

[14] Gopinath, A., Puhan, S., Nagarajan, G., 2010. Effect of unsaturated fatty acid esters of biodiesel fuels on combustion, performance and emission characteristics of a DI diesel engine. Int. J. Energy Environ. 1(3), 411-430.

[15] Gupta, J., Agarwal, M., 2016. Preparation and characterizaton of CaO nanoparticle for biodiesel production. AIP Conf. Proc. 1724(1), 020066.

[16] Hellier, P., Talibi, M., Eveleigh, A., Ladommatos, N., 2017. An overview of the effects of fuel molecular structure on the combustion and emissions characteristics of compression ignition engines. Proc. Inst. Mech. Eng., D. 232(1), 90-105.

[17] Kaisan, M.U., Anafi, F.O., Nuszkwoski, J., Kulla D.M., Umaru, S., 2016. GC/MS analysis of methyl esters of biodiesel produced from cotton seed oil. Niger. J. Sol. Energy. 27, 56-61.

[18] Kalz, K.F., Kraehnert, R., Dvoyashkin, M., Dittmeyer, R., Glaser, R., Krewer, U., Reuter, K., Grunwaldt, J.D., 2017. Future challenges in heterogeneous catalysis: understanding catalysts under dynamic reaction conditions. ChemCatChem. 9(1), 17-29.

[19] Kamal, N.B.T.M., 2018. Preparation, characterization and mechanistic study of alumina supported calcium oxide based catalysts in transesterification of refined cooking oil. PhD Thesis, Universiti Teknologi Malaysia, Malaysia.

[20] Kwong, T., Yung, K., 2015. Heterogeneous alkaline earth metal-transition metal bimetallic catalysts for synthesis of biodiesel from low grade unrefined feedstock. RSC Adv. 5(102), 83748-83756.

[21] Lapuerta, M., Armas, O., Rodríguez-Fernández, J., 2009. Effect of the Degree of Unsaturation of Biodiesel Fuels on NO_x and Particulate Emissions. SAE Int. J. Fuels Lubr. 1(1), 1150-1158.

[22] Mofijur, M., Rasul, M.G., Hassan, N.M.S., Masjuki, H.H., Kalam, M.A., Mahmudul, H.M., 2017. Chapter fourteen - assessment of physical, chemical, and tribological properties of different biodiesel Fuels. Clean Energy Sust. Dev. 441-463.

[23] Muthukumar, H., Matheswaran, M., 2015. *Amaranthus spinosus* leaf extract mediated FeO nanoparticles: physicochemical traits, photocatalytic and antioxidant activity. ACS Sust. Chem. Eng. 3(12), 3149-3156.

[24] Nasar, M., Taufiq-Yap, Y.H., 2017. Synthesis and characterization of solid heterogeneous catalyst for the production of biodiesel from high FFA waste cooking oil. Bayer. J. Pure Appl. Sci. 10(1), 62-66.

[25] Omotoso, M., Ayodele, M., Akintudire, A., 2011. Comparative Study of the properties of biodiesel prepared from *Jatropha curcas* oil and palm oil. Global Res. J. 1(1), 1-13.

[26] Prabu, M., Manikandan, M., Kandasamy, P., Kalaivani, P.R., Rajendiran, N., Raja, T., 2019. Synthesis of Biodiesel using the Mg/Al/Zn Hydrotalcite/SBA-15 Nanocomposite Catalyst. ACS Omega. 4(2), 3500-3507.

[27] Refaat, A.A., 2009. Correlation between the chemical structure of biodiesel and its physical properties. Int. J. Environ. Sci. Technol. 6(4), 677-694.

[28] Sharma, S., Saxena, V., Baranwal, A., Chandra, P., Pandey, L.M., 2018. Engineered nanoporous materials mediated heterogeneous catalysts and their implications in biodiesel production. Mater. Sci. Energy Technol. 1(1), 11-21.

[29] Sharmila, S., Rebecca, L.J., Anbuselvi, S., Kowsalya, E., Kripanand, N.R., 2016. GC-MS Analysis of biofuel extracted from marine algae. Der Pharmacia Lett. 8(3), 204-214.

[30] Sokoto, M.A., Hassan, L.G., Dangoggo, S.M., Ahmad, H.G., Uba, A., 2011. Influence of fatty acid methyl esters on fuel properties of biodiesel produced from the seeds oil of *Curcubita pepo*. Niger. J. Basic Appl. Sci. 19(1), 81-86.

[31] Sutapa, I. W., Wahab, A.W., Taba, P., Nafie, N., 2018. Synthesis and structural profile analysis of the MgO nanoparticles produced through the sol-gel method followed by annealing process. Orient. J. Chem. 34(2), 1016-1025.

[32] Tsai, C., 2017. Rational design of heterogeneous catalysts from first principles. PhD Thesis, Stanford University, California.

[33] Wang, Z., Hu, P., 2016. Towards rational catalyst design: a general optimization framework. Philos. Trans. R. Soc. London, Ser. A. 374(2061), 20150078.

[34] Yang, J., Astatkie, T., He, Q.S., 2016. A comparative study on the effect of unsaturation degree of camelina and canola oils on the optimization of bio-diesel production. Energy Rep. 2, 211-217.

[35] Yang, R., Du, X., Zhang, X., Xin, H., Zhou, K., Li, D., Hu, C., 2019. Transformation of Jatropha Oil into High-Quality Biofuel over Ni–W Bimetallic Catalysts. ACS Omega. 4(6), 10580-10592.

[36] Yin, W., Venderbosch, R.H., He, S., Bykova, M.V., Khromova, S.A., Yakovlev, V.A., Heeres, H.J., 2017. Mono-, bi-, and tri-metallic Ni-based catalysts for the catalytic hydrotreatment of pyrolysis liquids. Biomass Convers. Biorefin. 7(3), 361-376.

Please cite this article as: Aderibigbe F.A., Mustapha S.I., Adewoye T.L., Mohammed I.A., Gbadegesin A.B., Niyi F.E., Olowu O.I., Soretire A.G., Saka H.B. Qualitative role of heterogeneous catalysts in biodiesel production from *Jatropha curcas* oil. Biofuel Research Journal 26 (2020) 1159-1169. DOI: 10.18331/BRJ2020.7.2.4

Supplementary Data

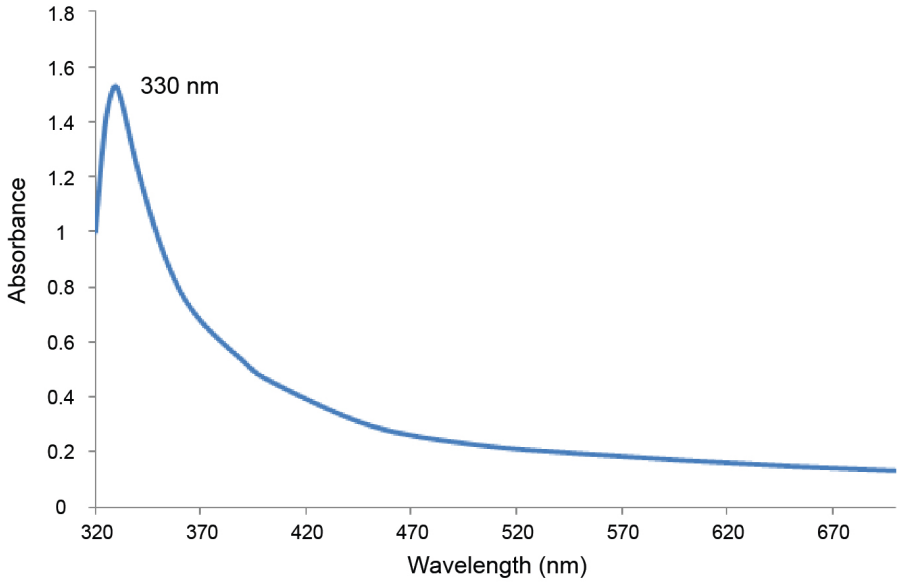


Fig. S1. FTIR spectrum of *Amaranthus spinosus* leaf extract.

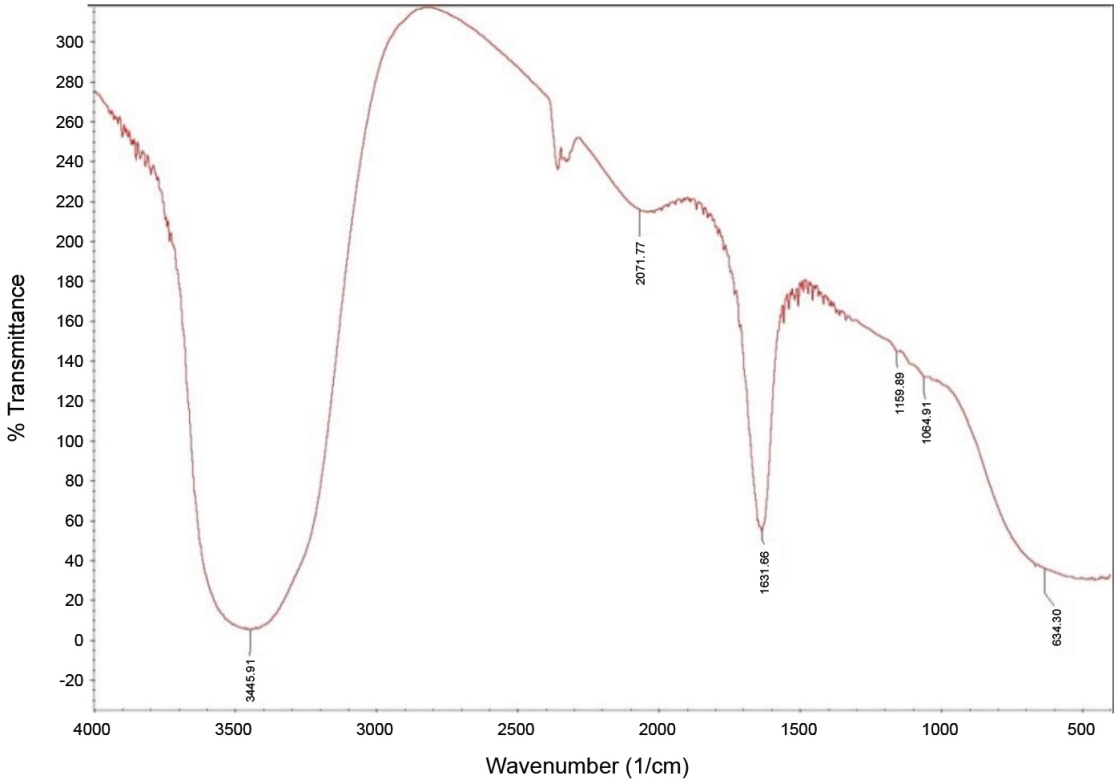


Fig. S2. UV-Vis spectrum of colloidal MgO nanoparticles

Please cite this article as: Aderibigbe F.A., Mustapha S.I., Adewoye T.L., Mohammed I.A., Gbadegesin A.B., Niyi F.E., Olowu O.I., Soretire A.G., Saka H.B. Qualitative role of heterogeneous catalysts in biodiesel production from *Jatropha curcas* oil. Biofuel Research Journal 26 (2020) 1159-1169. DOI: 10.18331/BRJ2020.7.2.4

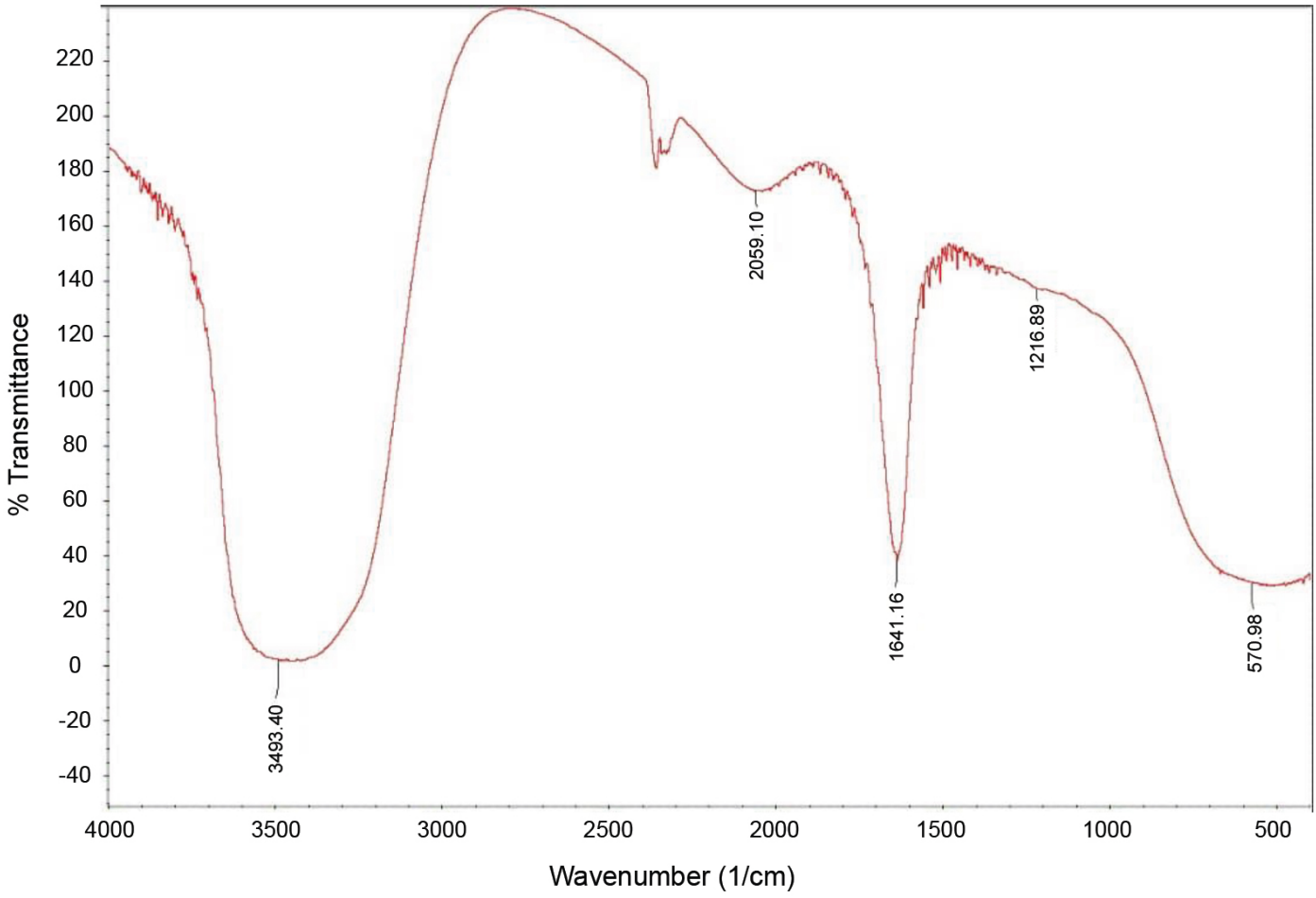


Fig. S3. FTIR spectrum of *Citrus aurantifolia* leaf extract.

Please cite this article as: Aderibigbe F.A., Mustapha S.I., Adewoye T.L., Mohammed I.A., Gbadegesin A.B., Niyi F.E., Olowu O.I., Soretire A.G., Saka H.B. Qualitative role of heterogeneous catalysts in biodiesel production from *Jatropha curcas* oil. Biofuel Research Journal 26 (2020) 1159-1169. DOI: 10.18331/BRJ2020.7.2.4

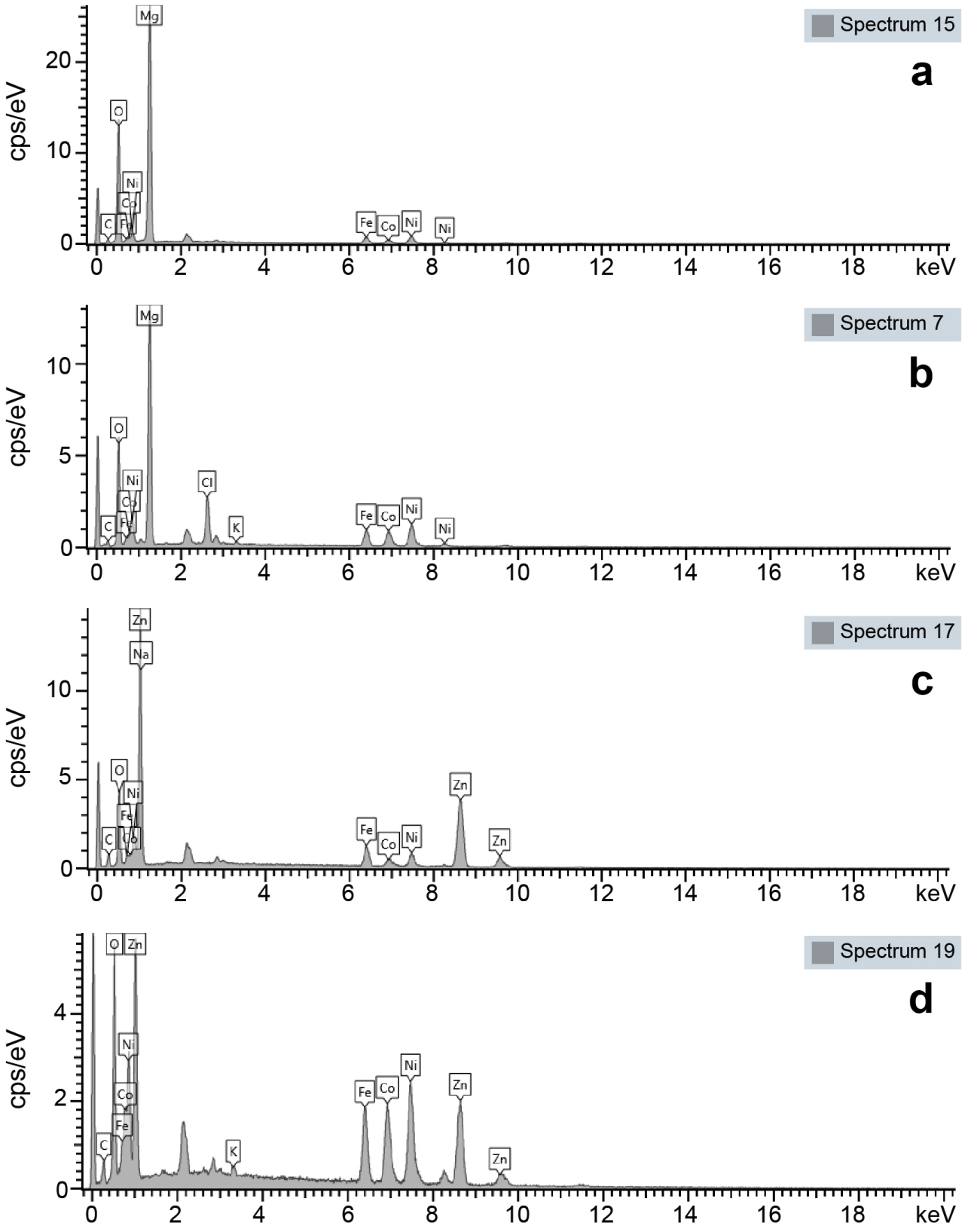


Fig. S4. The EDS analysis of different catalysts; (a) *Fe-Co-Ni/MgO*, (b) *Fe-Co-Ni-MgO*, (c) *Fe-Co-Ni/ZnO*, and (d) *Fe-Co-Ni-ZnO*.

Please cite this article as: Aderibigbe F.A., Mustapha S.I., Adewoye T.L., Mohammed I.A., Gbadegesin A.B., Niyi F.E., Olowu O.I., Soretire A.G., Saka H.B. Qualitative role of heterogeneous catalysts in biodiesel production from *Jatropha curcas* oil. Biofuel Research Journal 26 (2020) 1159-1169. DOI: 10.18331/BRJ2020.7.2.4

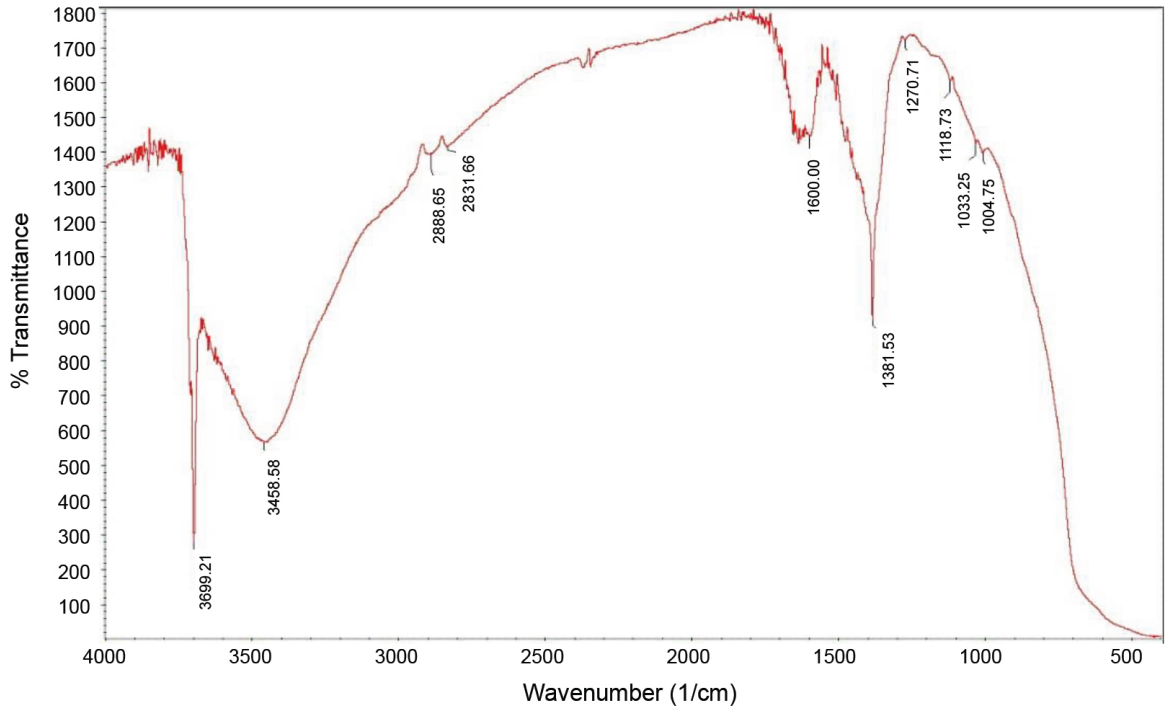


Fig. S5. FTIR spectrum of *Fe-Co-Ni/MgO* catalyst.

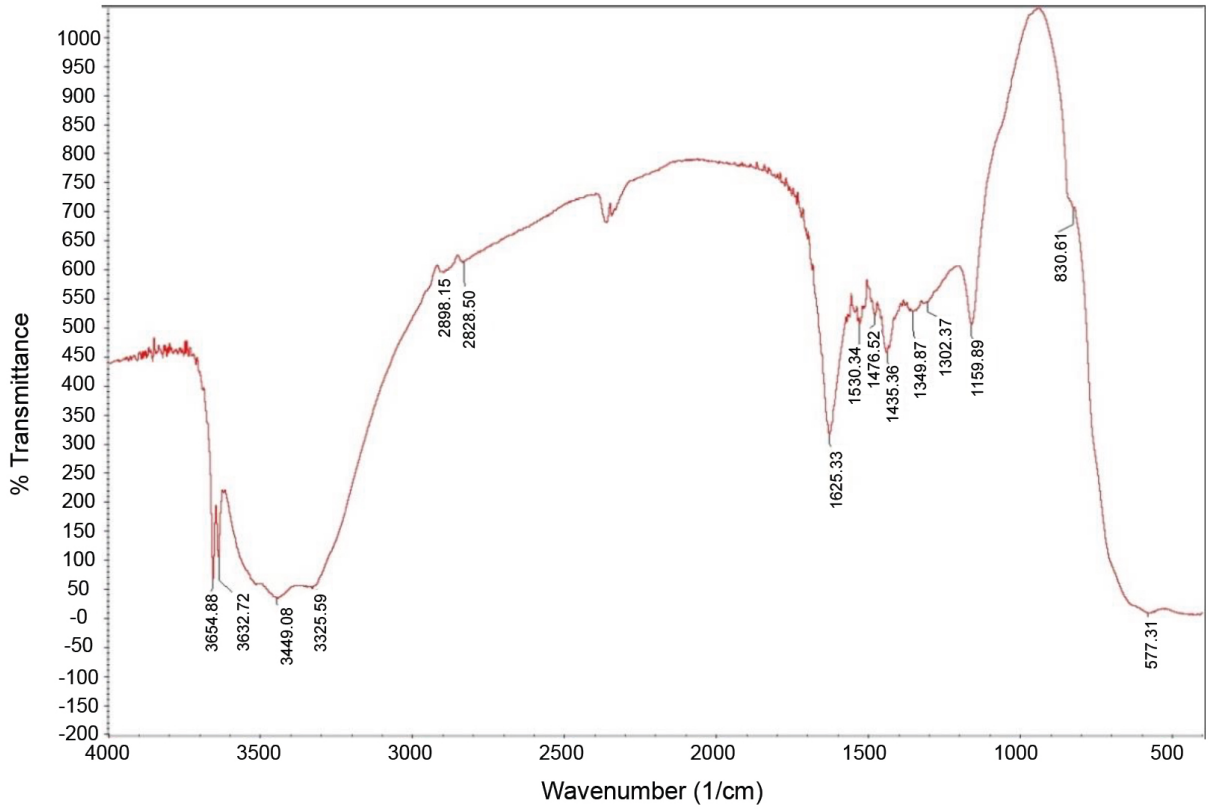


Fig. S6. FTIR spectrum of *Fe-Ni-Co-MgO* catalyst.

Please cite this article as: Aderibigbe F.A., Mustapha S.I., Adewoye T.L., Mohammed I.A., Gbadegesin A.B., Niyi F.E., Olowu O.I., Soretire A.G., Saka H.B. Qualitative role of heterogeneous catalysts in biodiesel production from *Jatropha curcas* oil. Biofuel Research Journal 26 (2020) 1159-1169. DOI: 10.18331/BRJ2020.7.2.4

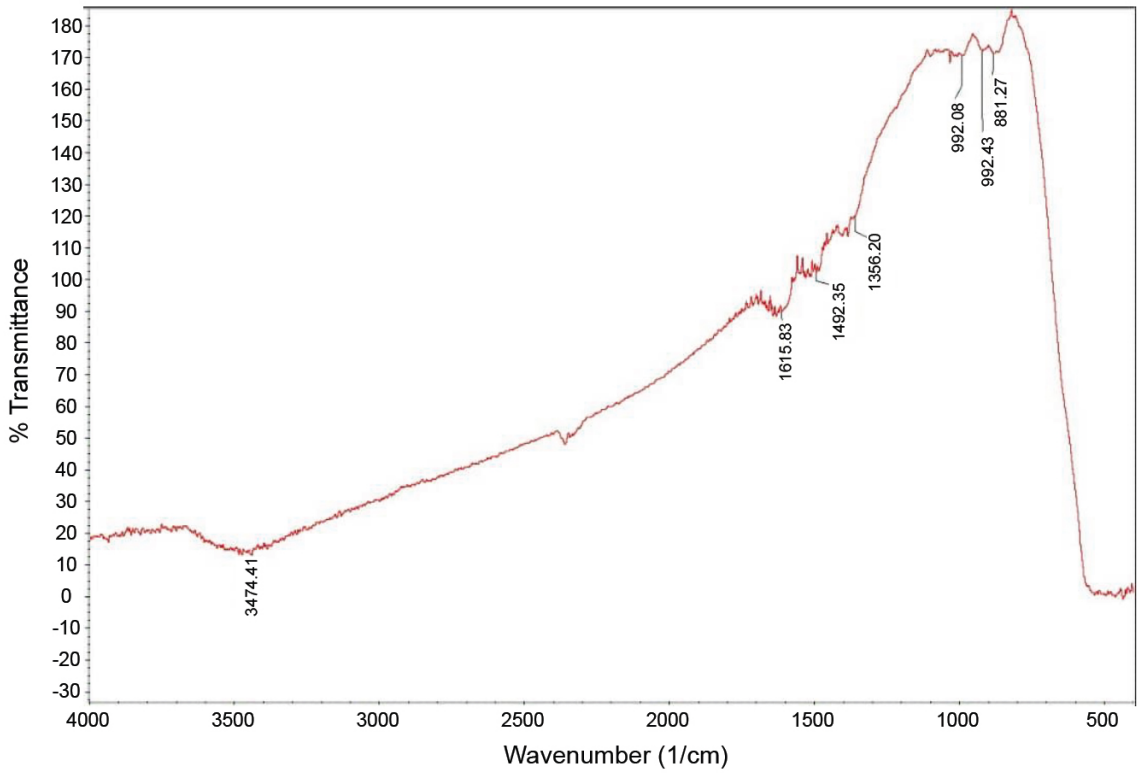


Fig. S7. FTIR spectrum of *Fe-Co-Ni/ZnO* catalyst.

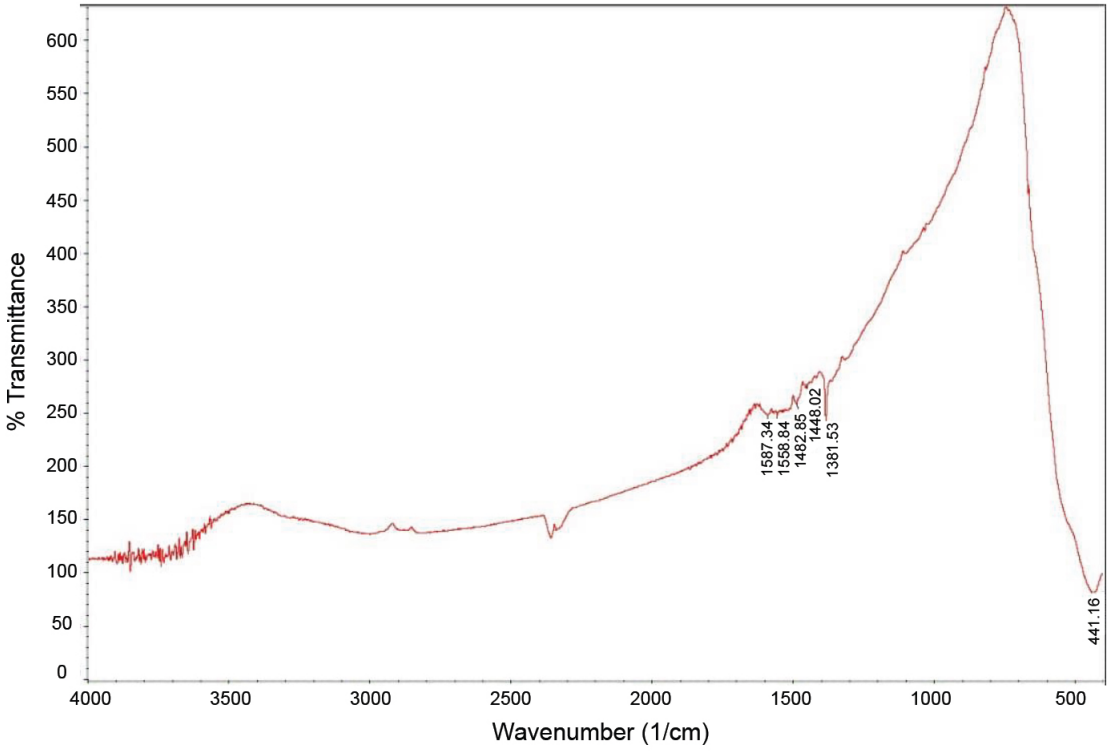


Fig. S8. FTIR spectrum of *Fe-Ni-Co-ZnO* catalyst.

Please cite this article as: Aderibigbe F.A., Mustapha S.I., Adewoye T.L., Mohammed I.A., Gbadegesin A.B., Niyi F.E., Olowu O.I., Soretire A.G., Saka H.B. Qualitative role of heterogeneous catalysts in biodiesel production from *Jatropha curcas* oil. Biofuel Research Journal 26 (2020) 1159-1169. DOI: 10.18331/BRJ2020.7.2.4

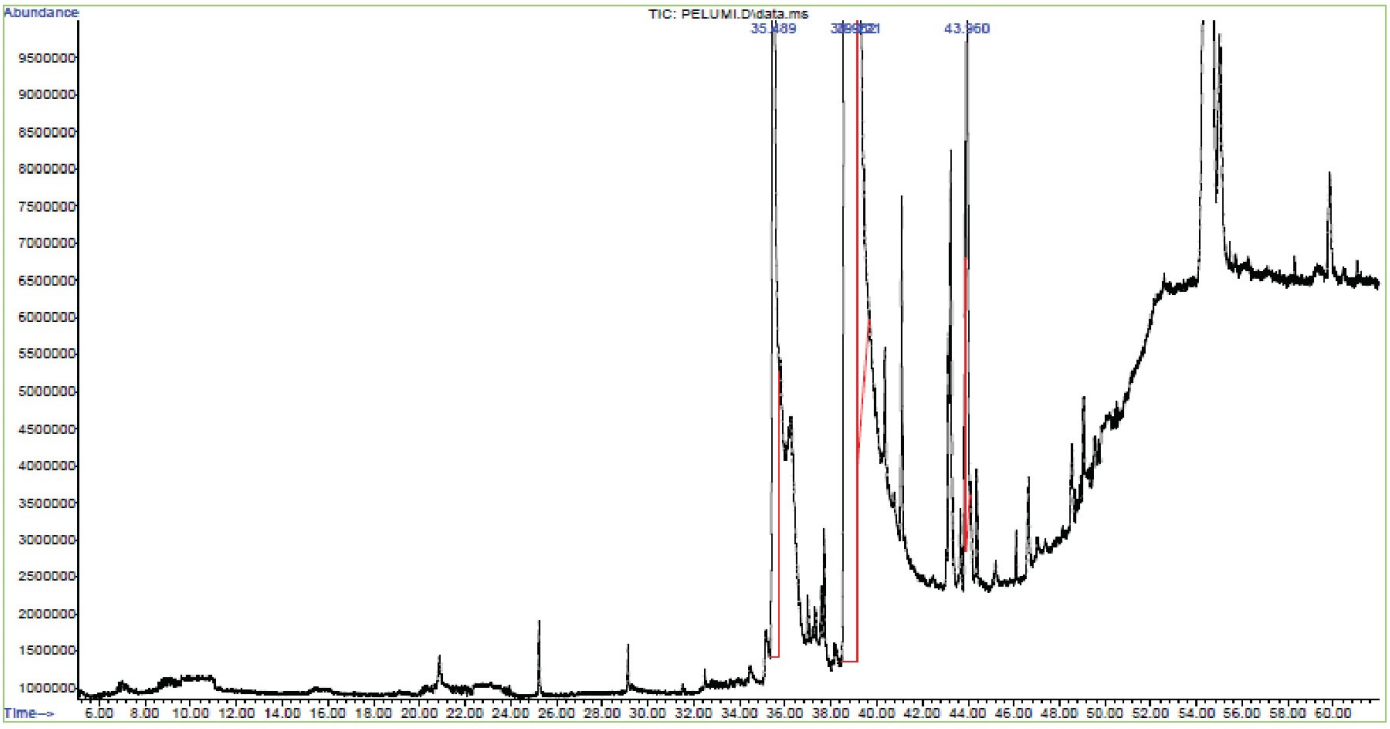


Fig. S9. FAME profile of the biodiesel produced by *Fe-Co-Ni/MgO*.

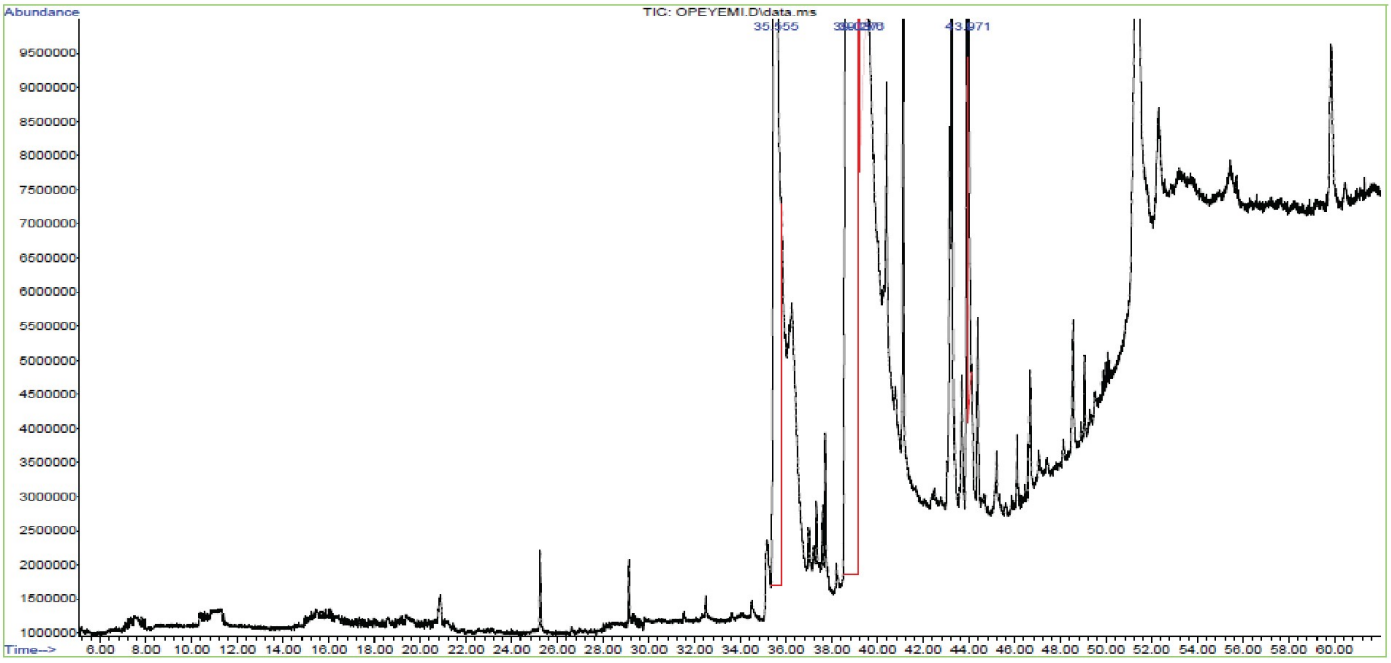


Fig. S10. FAME profile of the biodiesel produced by *Fe-Co-Ni-MgO*.

Please cite this article as: Aderibigbe F.A., Mustapha S.I., Adewoye T.L., Mohammed I.A., Gbadegesin A.B., Niyi F.E., Olowu O.I., Soretire A.G., Saka H.B. Qualitative role of heterogeneous catalysts in biodiesel production from *Jatropha curcas* oil. Biofuel Research Journal 26 (2020) 1159-1169. DOI: 10.18331/BRJ2020.7.2.4

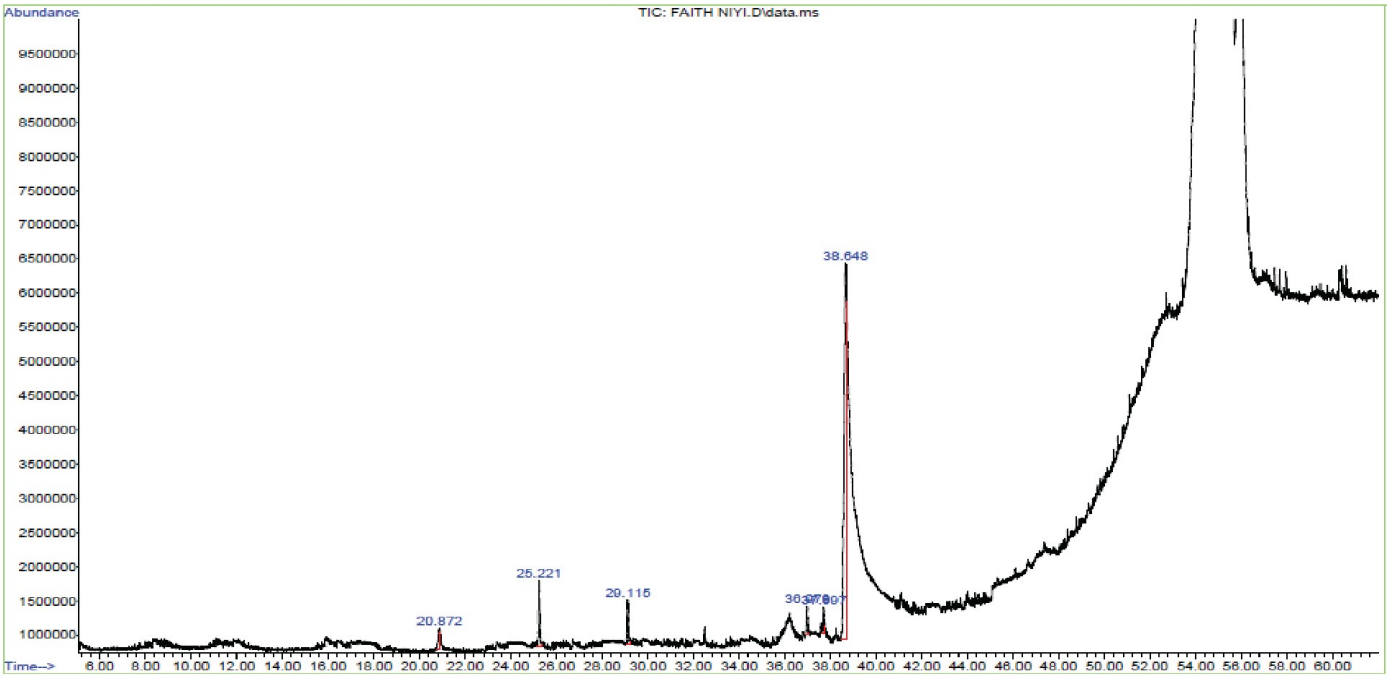


Fig. S11. FAME profile of the biodiesel produced by *Fe-Co-Ni/ZnO*.

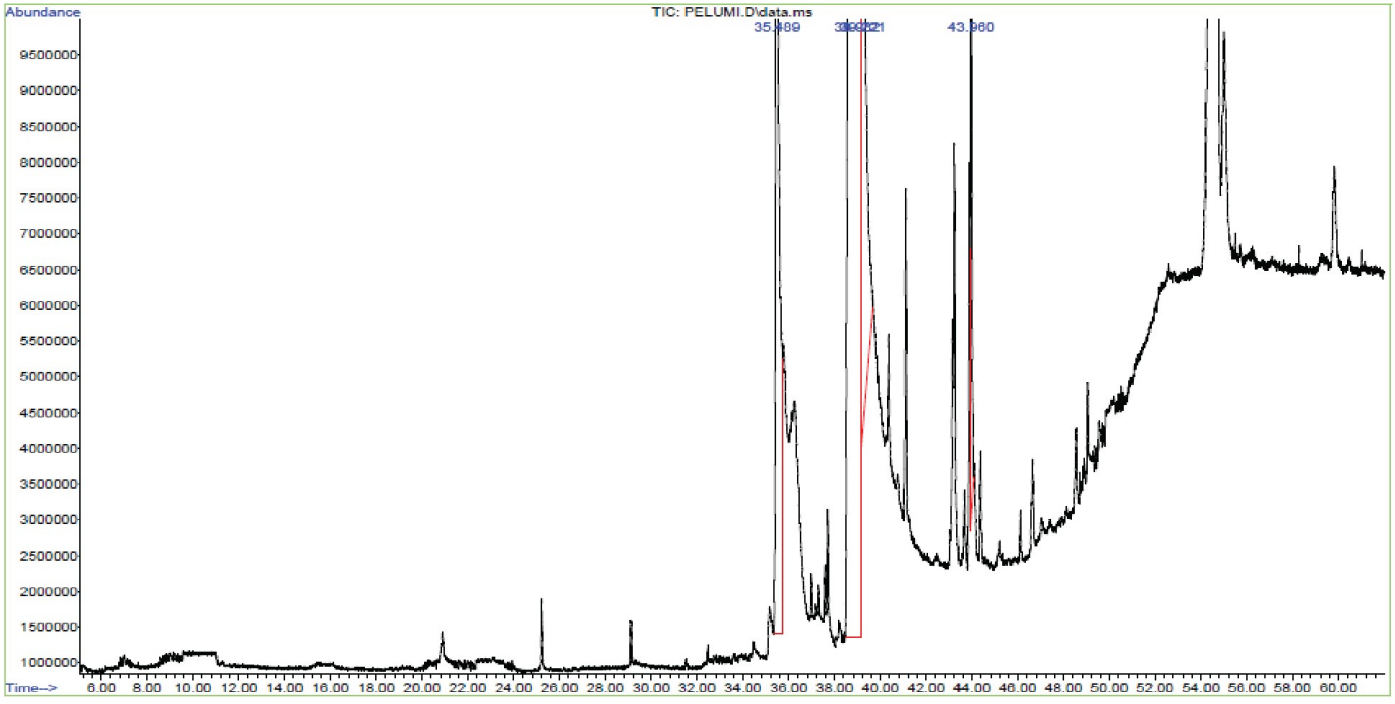


Fig. S12. FAME profile of the biodiesel produced by *Fe-Co-Ni-ZnO*.

Please cite this article as: Aderibigbe F.A., Mustapha S.I., Adewoye T.L., Mohammed I.A., Gbadegesin A.B., Niyi F.E., Olowu O.I., Soretire A.G., Saka H.B. Qualitative role of heterogeneous catalysts in biodiesel production from *Jatropha curcas* oil. Biofuel Research Journal 26 (2020) 1159-1169. DOI: 10.18331/BRJ2020.7.2.4

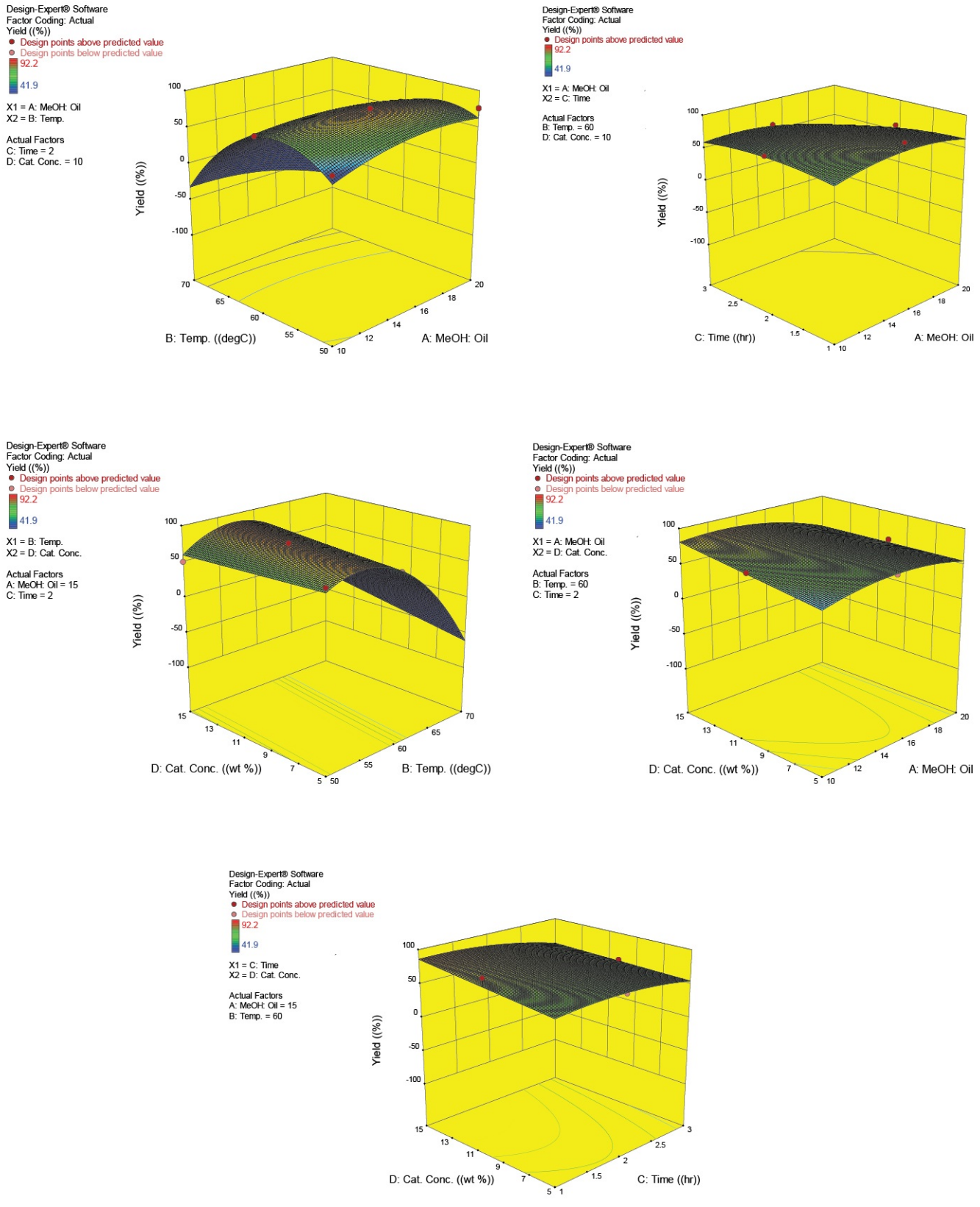


Fig. S13. Interactive effects of the transesterification parameters using *Fe-Co-Ni/MgO*.

Please cite this article as: Aderibigbe F.A., Mustapha S.I., Adewoye T.L., Mohammed I.A., Gbadegesin A.B., Niyi F.E., Olowu O.I., Soretire A.G., Saka H.B. Qualitative role of heterogeneous catalysts in biodiesel production from *Jatropha curcas* oil. Biofuel Research Journal 26 (2020) 1159-1169. DOI: 10.18331/BRJ2020.7.2.4

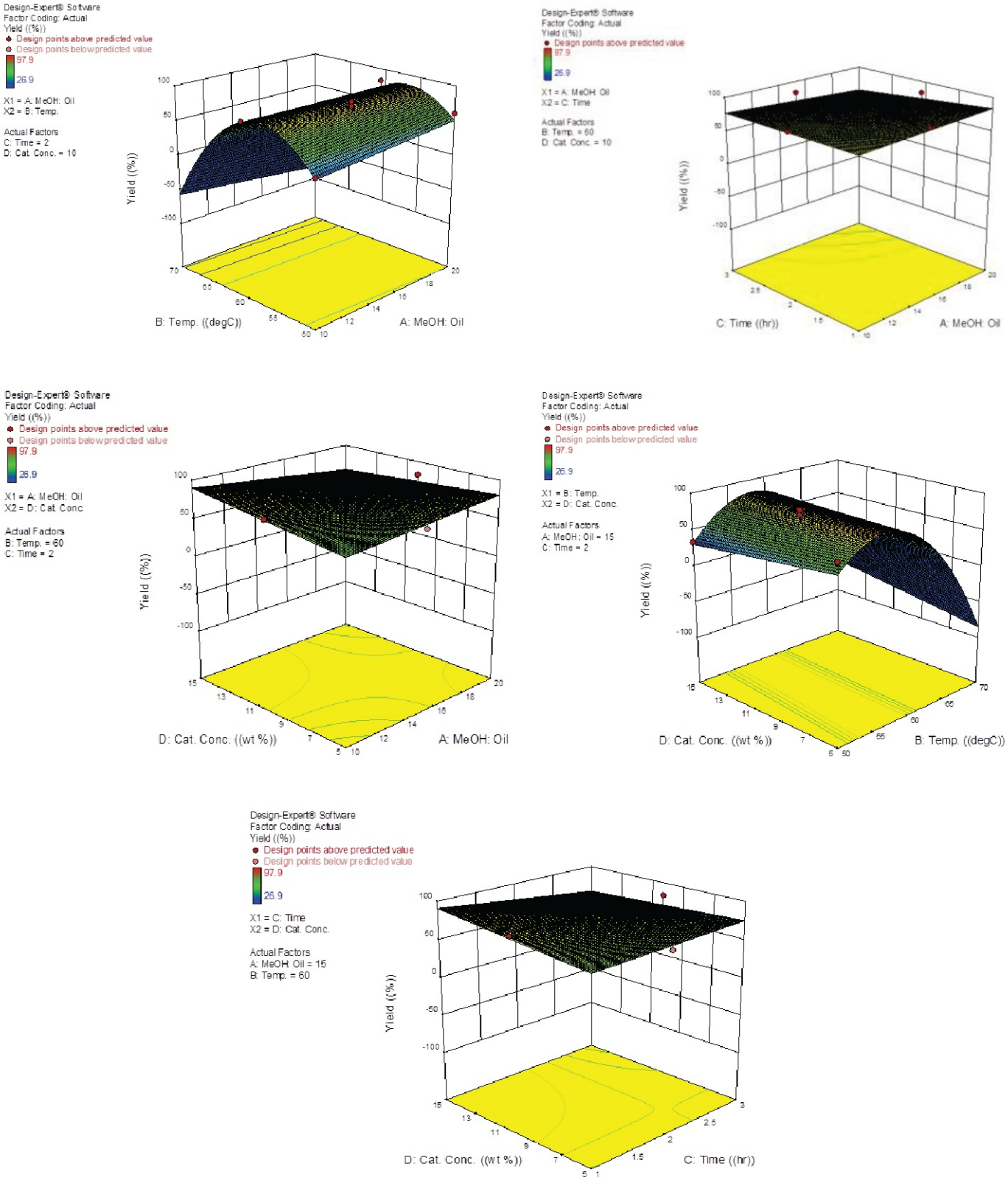


Fig. S14. Interactive effects of the transesterification parameters using *Fe-Co-Ni-MgO*.

Please cite this article as: Aderibigbe F.A., Mustapha S.I., Adewoye T.L., Mohammed I.A., Gbadegesin A.B., Niyi F.E., Olowu O.I., Soretire A.G., Saka H.B. Qualitative role of heterogeneous catalysts in biodiesel production from *Jatropha curcas* oil. Biofuel Research Journal 26 (2020) 1159-1169. DOI: 10.18331/BRJ2020.7.2.4

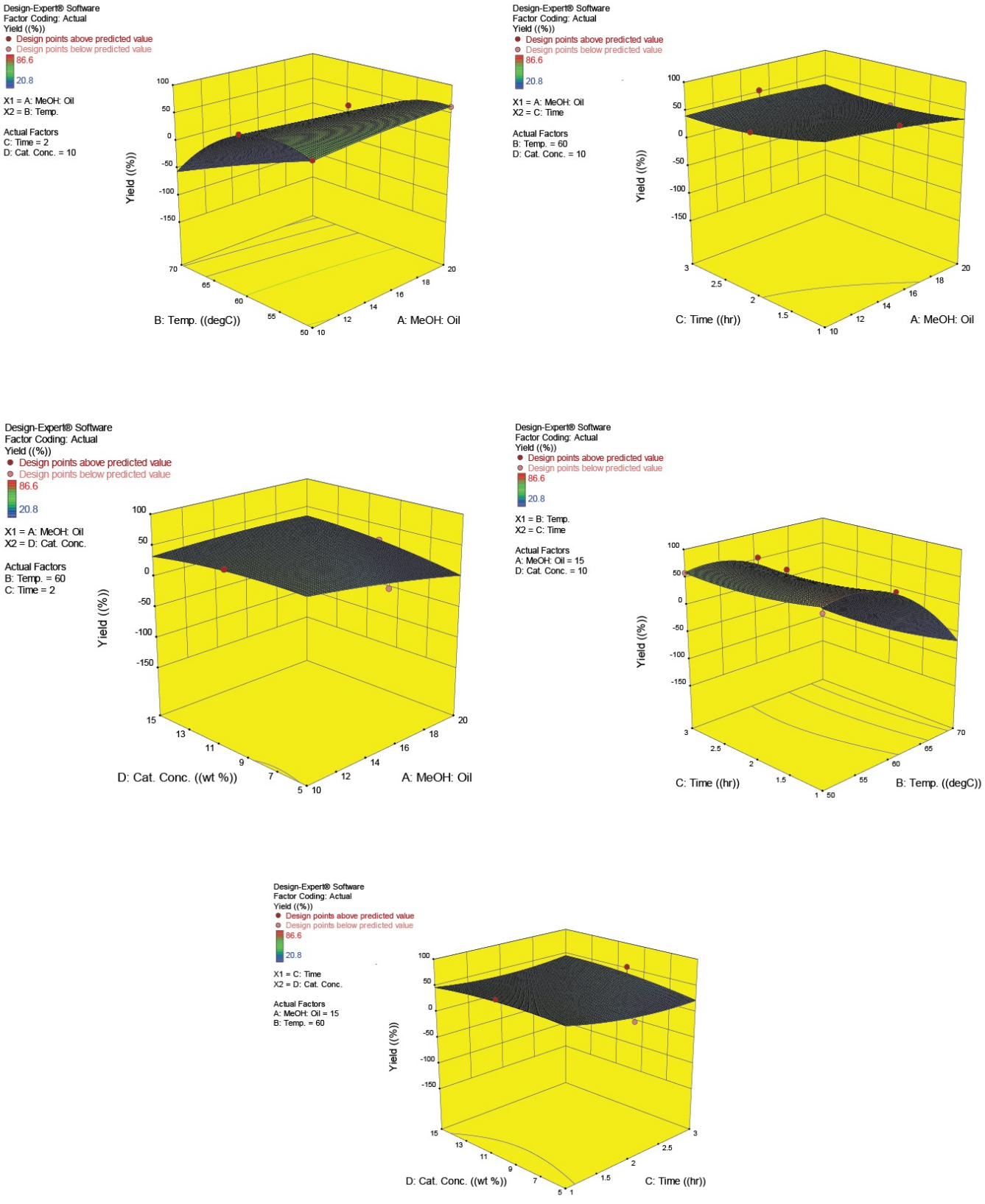


Fig. S15. Interactive effects of the transesterification parameters using *Fe-Co-Ni/ZnO*.

Please cite this article as: Aderibigbe F.A., Mustapha S.I., Adewoye T.L., Mohammed I.A., Gbadegesin A.B., Niyi F.E., Olowu O.I., Soretire A.G., Saka H.B. Qualitative role of heterogeneous catalysts in biodiesel production from *Jatropha curcas* oil. Biofuel Research Journal 26 (2020) 1159-1169. DOI: 10.18331/BRJ2020.7.2.4

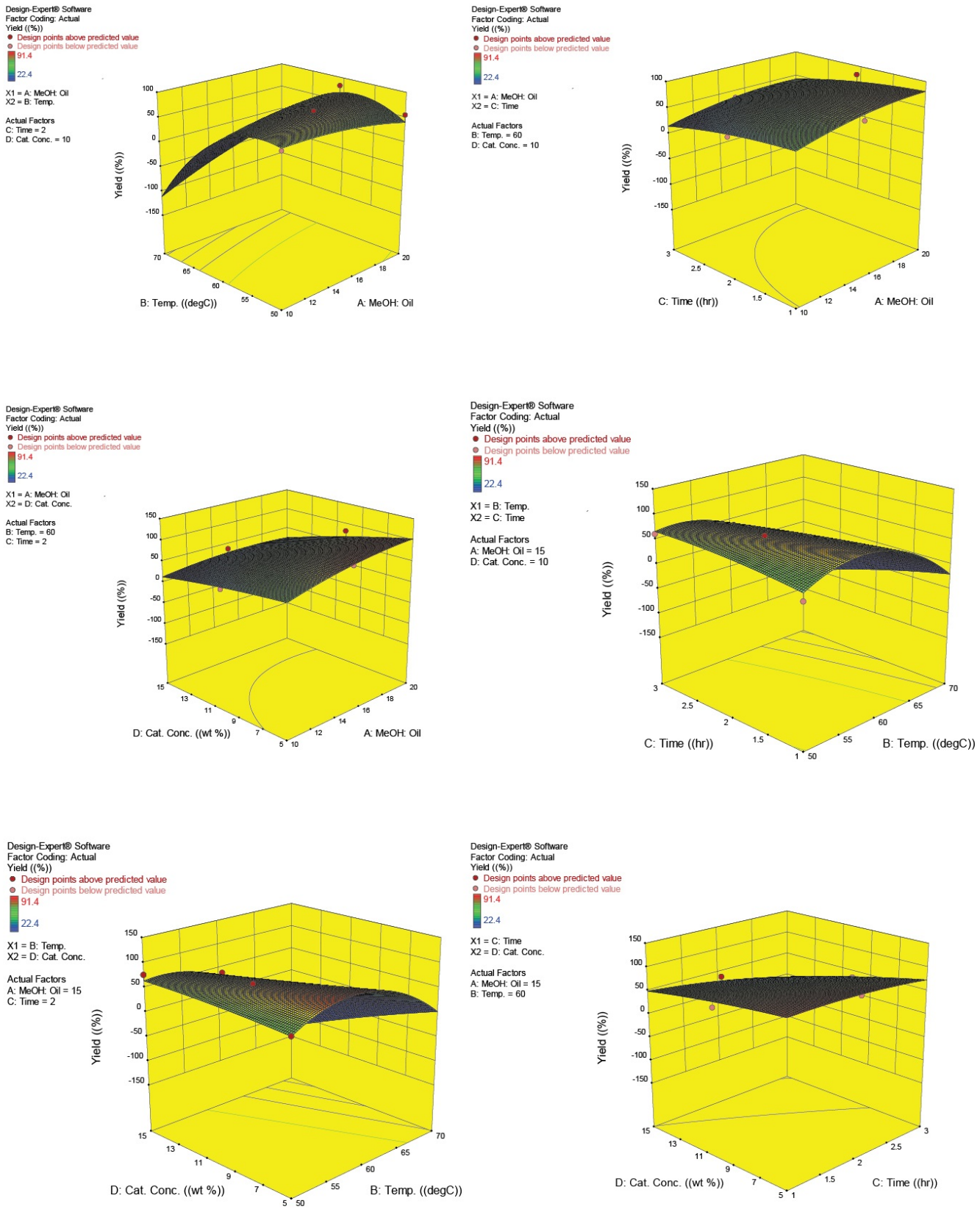


Fig. S16. Interactive effects of the transesterification parameters using *Fe-Co-Ni-ZnO*.

Please cite this article as: Aderibigbe F.A., Mustapha S.I., Adewoye T.L., Mohammed I.A., Gbadegesin A.B., Niyi F.E., Olowu O.I., Soretire A.G., Saka H.B. Qualitative role of heterogeneous catalysts in biodiesel production from *Jatropha curcas* oil. Biofuel Research Journal 26 (2020) 1159-1169. DOI: 10.18331/BRJ2020.7.2.4